

Article

Appraisal of Land Cover and Climate Change Impacts on Water Resources: A Case Study of Mohmand Dam Catchment, Pakistan

Muhammad Umer Masood ¹, Noor Muhammad Khan ², Saif Haider ¹, Muhammad Naveed Anjum ^{3,*}, Xi Chen ^{4,5}, Aminjon Gulakhmadov ^{4,5,6,*}, Mudassar Iqbal ¹, Zeshan Ali ¹ and Tie Liu ⁵

¹ Centre of Excellence in Water Resources Engineering, University of Engineering and Technology, Lahore 54890, Pakistan

² Department of Civil Engineering, University of Engineering and Technology, Lahore 54890, Pakistan

³ Department of Land and Water Conservation Engineering, Faculty of Agricultural Engineering and Technology, PMAS-Arid Agriculture University, Rawalpindi 46000, Pakistan

⁴ Research Center for Ecology and Environment of Central Asia, Xinjiang Institute of Ecology and Geography, Chinese Academy of Sciences, Urumqi 830011, China

⁵ State Key Laboratory of Desert and Oasis Ecology, Xinjiang Institute of Ecology and Geography, Chinese Academy of Sciences, Urumqi 830011, China

⁶ Institute of Water Problems, Hydropower and Ecology of the National Academy of Sciences of Tajikistan, Dushanbe 734042, Tajikistan

* Correspondence: naveedwre@uaar.edu.pk (M.N.A.); aminjon@ms.xjb.ac.cn (A.G.)

Abstract: Land cover change (LCC) and climate change (CC) impacts on streamflow in high elevated catchments are a great challenge to sustainable management and the development of water resources. This study evaluates the possible future impacts of both land cover and climate change on the streamflows in the Mohmand Dam catchment, Pakistan, by utilizing the semi-distributed hydrological model known as the Soil and Water Assessment Tool (SWAT), along with the latest Coupled Model Intercomparison Project phase 6 (CMIP6) dataset of different global climate models (GCMs). The downscaling of the precipitation and temperature data was performed by the CMhyd software. The downscaled precipitation and temperature projections from the best performing GCM, out of four GCMs, under two shared socioeconomic pathways (SSP2 and SSP5) and future land cover conditions were forced in a calibrated hydrological model (SWAT model). Compared to the baseline period (1990–2015), the outputs from the selected GCM indicated an increase in the average monthly precipitation, and the maximum and minimum temperature in the study area under both the SSP2 and SSP5 scenarios, by the end of the 21st century. It is expected that the increase in precipitation for the period 2016–2100 is 10.5% and 11.4% under the SSP2 and SSP5 scenarios, respectively. Simulated results from the SWAT model showed significant impacts from the projected climate and land cover changes on Mohmand Dam flows that include: (a) an increase in the overall mean annual flow ranging from 13.7% to 34.8%, whereas the mean monthly flows of June, July and August decreased, and (b) a shift in the peak flows in the Mohmand catchment from July to June. It is concluded that the projected climate changes can substantially influence the seasonality of flows at the Mohmand Dam site. Climate and land cover change impacts are significant, so project planners and managers must include CC and LCC impacts in the proposed operational strategy.



Citation: Masood, M.U.; Khan, N.M.; Haider, S.; Anjum, M.N.; Chen, X.; Gulakhmadov, A.; Iqbal, M.; Ali, Z.; Liu, T. Appraisal of Land Cover and Climate Change Impacts on Water Resources: A Case Study of Mohmand Dam Catchment, Pakistan. *Water* **2023**, *15*, 1313. <https://doi.org/10.3390/w15071313>

Academic Editor: Chuanzhe Li

Received: 8 February 2023

Revised: 23 March 2023

Accepted: 24 March 2023

Published: 27 March 2023



Copyright: © 2023 by the authors. Licensee MDPI, Basel, Switzerland. This article is an open access article distributed under the terms and conditions of the Creative Commons Attribution (CC BY) license (<https://creativecommons.org/licenses/by/4.0/>).

Keywords: climate change; land use classification; statistical downscaling; land cover change; Mohmand Dam; GCMs

1. Introduction

For the production of food, the generation of electricity and the sustainable development of any nation, a stable water supply is essential [1]. More than half of the world's water needs are being met by rivers [2]. However, river flows are susceptible to long-term

changes in temperature and precipitation, especially in areas where flows are dominated by snowmelt [3,4]. Variations in precipitation typically have an impact on the amount of snow that accumulates, which can ultimately have an impact on runoff volume, whereas variations in temperature typically have an impact on the seasonality of the water supply [5,6].

The Hindukush, Karakoram and Himalaya (HKH) mountainous region has a significant impact on both the Asian and global atmospheric circulation systems, due to its tall mountains and vast cryospheric area [7]. Excessive groundwater pumping is leading to negative agro-economic effects [8,9]. The sub-basins of the UIB undergo several atmospheric circulation systems, with the southeast monsoon circulation system having a strong influence on the southeastern (SE) half and the westerlies disturbances having a significant impact on the Hindukush range (Gilgit, Chitral and Swat) [10–15]. The temperature at the UIB is consistently rising, but the rate of this rise varies among the sub-basins [15–25]. Sub-basins controlled by the monsoon exhibit a persistent decline in precipitation, while high-altitude sub-basins located in westerly dominated belts have not seen a clear trend of increasing or decreasing precipitation [13,16,24–26]. To anticipate future water resources in the context of climate change, it is necessary to examine the projected effects of climate change on the future hydrological responses at the sub-basin scale. GCMs are the most sophisticated coupled numerical models for predicting the general circulation of the Earth's atmosphere, but their coarse spatial resolutions make them less accurate at the basin scale [27–34]. Statistical or dynamic downscaling (DD) techniques are used to downscale the outputs of GCMs, to make them appropriate and representative [31]. SWAT is a powerful modeling tool that can be used to assess the impact of climate change and land use change on natural resources, such as soil, water and vegetation. SWAT can help identify areas where land use changes may have negative effects on water quality or soil health and inform decisions about how to manage land use in a sustainable manner. By using SWAT to model different scenarios and assess the potential impacts of various management strategies, researchers and decision-makers can develop more effective policies and practices for managing our natural resources in a changing world.

It is expected that the average annual temperature and precipitation in the UIB will rise by 0.3–4.8 °C and 19–113%, respectively, by the end of the 21st century [32]. This has led to a number of researchers predicting how future climate change may affect the hydrological responses of several sub-basins in the UIB, located in the Karakoram and Himalayan ranges [8,23,33–38]. For instance, Garee et al. [39] came to the conclusion that the Karakoram range's river flow might be 10% higher at the end of the century. According to Mahmood et al. [35], the Jhelum River watershed in the Himalayan range might see a 15% increase in its annual average river flow. There is a lack of literature describing the potential effects of land cover and climatic changes on the water resources of the UIB sub-basins located in the Hindukush Mountains. Moreover, simple (statistical) lumped models were employed to evaluate the hydrological response of the UIB sub-basins that were under study [35,37]. Rarely were the physical characteristics of the UIB's snowy or glaciated sub-basins described [39,40]. The Swat River basin, which has the highest water output available among all of the UIB sub-basins, has not yet been the subject of any studies that examine how future climate change would affect its hydrological response [14]. This study seeks to address the gap in the literature, by examining the effects of expected changes in precipitation, temperature and land cover attributes on the river flow of the Mohmand Dam catchment.

The primary scientific goals of this investigation were: (1) to assess historical water resource availability and land cover change trends for the Mohmand Dam catchment in Pakistan and (2) the assessment of probable impacts of climate and land cover change on the water resources of the Mohmand Dam catchment area using the output of GCMs under two different shared socioeconomic pathways (SSPs 2 and 5). Additionally, assessments were made of the temporal variations in peak flows, as well as previous and prospective changes in the land cover. Section 2 of this document discusses the data utilized in this investigation and the study area. The methodology of statistical downscaling used in this

study is briefly described in Section 3, along with the hydrological model (SWAT) and its calibration and validation. The findings and discussions are presented in Sections 4 and 5, while Section 6 provides the conclusions. The results of this inquiry will be beneficial to water resource managers, policy makers and hydrologists.

2. Study Area and Datasets

2.1. Study Area

The Mohmand Dam (also known as the Munda Dam) is under construction on the Swat River about 5 km upstream of the Munda Headworks, which is located about 48 km northeast of Peshawar (the provincial capital of Khyber Pakhtunkhwa). The total catchment area of the Swat River at the Mohmand Dam site is 13,956 km² (Figure 1). The Mohmand Dam will be located at latitude 34°21' N and longitude 71°32' E. The main purposes of the dam construction at Munda are the storage of water for irrigation and hydropower. In addition, flood mitigation will be an added benefit from the proposed dam. The Swat River joins the Kabul River at Charsadda, about 32 km downstream of the Munda Headworks, and is one of the main left bank tributaries of the Kabul River.

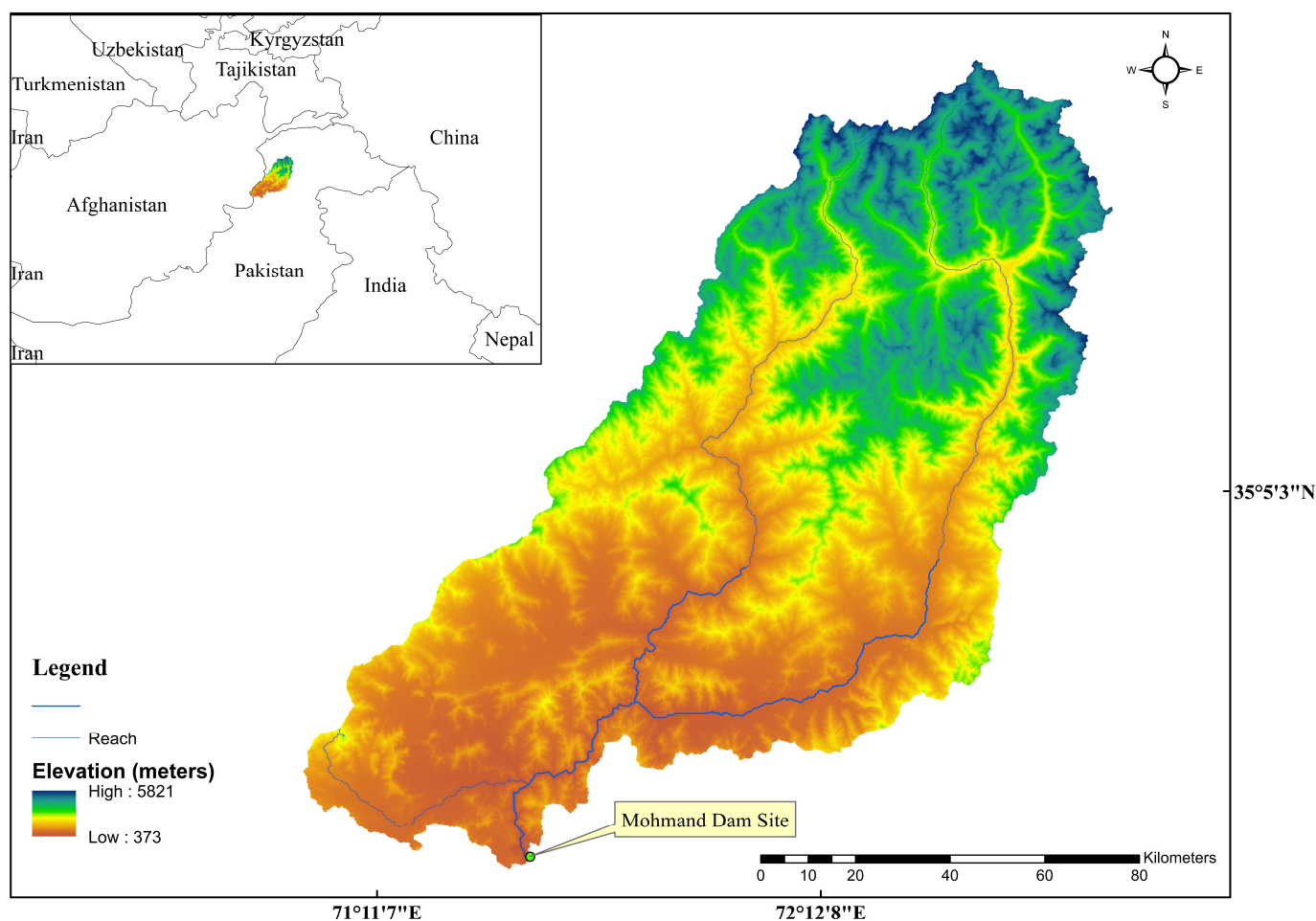


Figure 1. Location map of the Mohmand Dam catchment area.

The Swat River initiates in the Kalam through the confluence of the Gabral and Ushu Rivers. The Amandara and Panjkora Rivers are its primary tributaries, with a large number of minor left and right tributaries. From north to south, the catchment area is predominantly mountainous, with heights varying between 360–4500 m above the mean sea level. Annual rainfall averages between 375 mm and 1250 mm. Glaciers can be seen over 4000 m. Snowmelt has a significant impact on the runoff of the Swat River from May to June, while monsoons have an impact from July to September. The whole catchment

area of the proposed Mohmand Dam project is located between latitudes $34^{\circ}20' N$ and $35^{\circ}56' N$, and longitudes $70^{\circ}59' E$ and $72^{\circ}47' E$. Figure 1 shows the digital elevation model (DEM) of the catchment area on the map.

In the Swat River basin the annual average precipitation gradient runs from north to west, which shows that the spatial and temporal distribution of precipitation varies greatly over the study area [40]. The temperature of the basin ranges from moderate (in the north) to subtropical (in the southern parts). According to the most recent version (V06) of the Randolph Glacier Inventory (RGI 6.0), there are 512 glaciers overall in the Swat River basin and the total percentage of the glaciated area in the Swat basin is approximately 2.54%. Snowmelt dominates the river discharge in the northern portion of the basin, while liquid precipitation (rainfall) provides the majority of the flow in the southern portion [16,23]. Particularly in the northern regions of the basin, the majority of the winter precipitation in the region takes the form of snow. The Swat River at the Chakdara gauge has a mean annual discharge of 193 cumecs measured at the exit of the basin, based on 54 years (1964–2015) of river flow data provided by Water and Power Development Authority (WAPDA). Peak discharge is known to occur around July. Figure 2 shows the yearly maximum temperature, yearly minimum temperature and annual precipitation gradient.

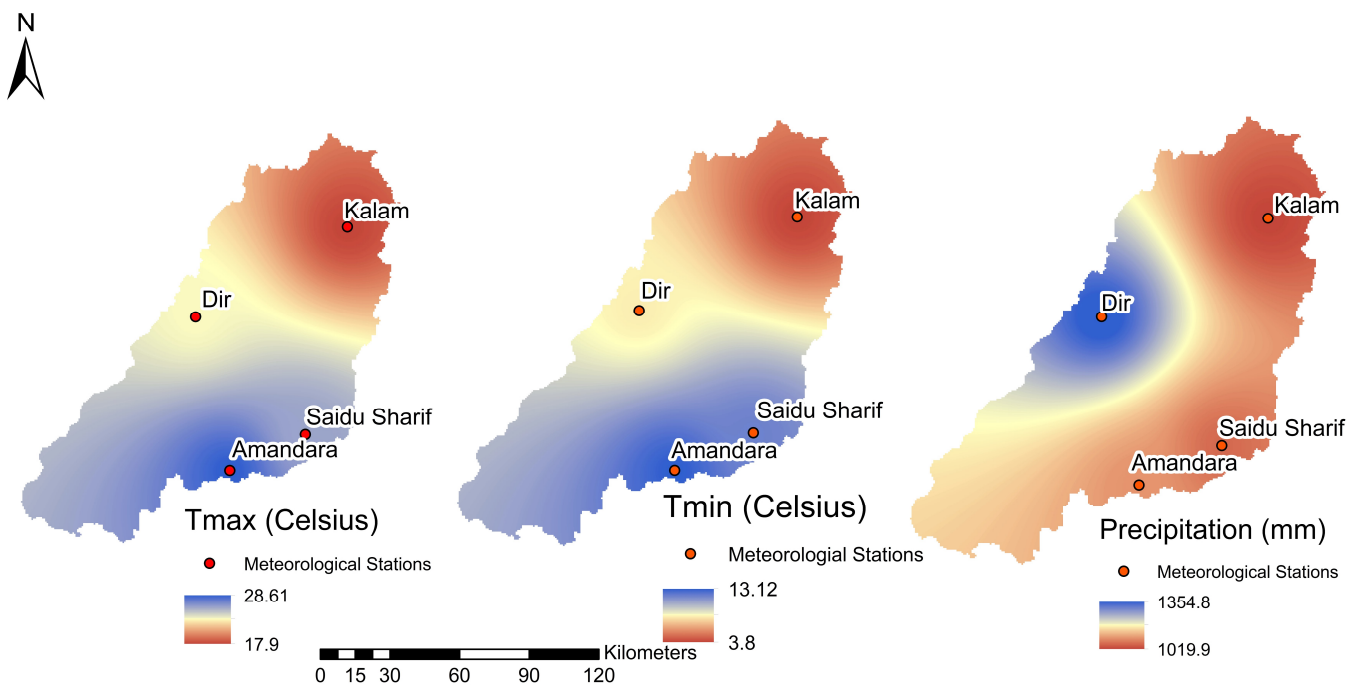


Figure 2. Yearly maximum temperature, yearly minimum temperature and annual precipitation gradient.

2.2. Datasets

2.2.1. Soil Data

Soil data is considered as a significant input variable for SWAT model setup. For this model, many types of soil surface texture, chemical and physical properties, including bulk density, the hydraulic conductivity of the soil and the available moisture content (AMC) are required. The IPCC Global soil classification dataset was used to prepare the soil map of the area. A total of seven soil classes were observed in the Mohmand Dam catchment area as shown in Figure 2. Other details of these classes, such as soil name, texture and distribution of the soil in the study area, are given in Table 1. As observed in Figure 3, Lithosols (I-B-U-2c) soil is the prominent soil type, as it covers 46.7% of the total catchment area, followed by Eutric Cambisols that covers 32% of the total area.

Table 1. Statistics on the soil distribution in the Mohmand Dam catchment area.

Sr. No.	Soil	Name	Texture	Area (km ²)	Weightage of Area
1	I-B-U-2c-3503	Lithosols	LOAM	6517.53	46.7
2	I-X-c-3512	Lithosols	LOAM	919.52	6.6
3	Be70-2-3a-3667	Haloic Cambisols	CLAY_LOAM	1043.86	7.5
4	Be73-2c-3673	Eutric Cambisols	LOAM	4464.06	32.0
5	I-B-U-3712	Calcaric Fluvisol	LOAM	523.71	3.8
6	Xh18-bc-3870	Haplic Xerosols	SILT_LOAM	220.86	1.6
7	GLACIER-6998	Gleysols	UWB	266.75	1.9

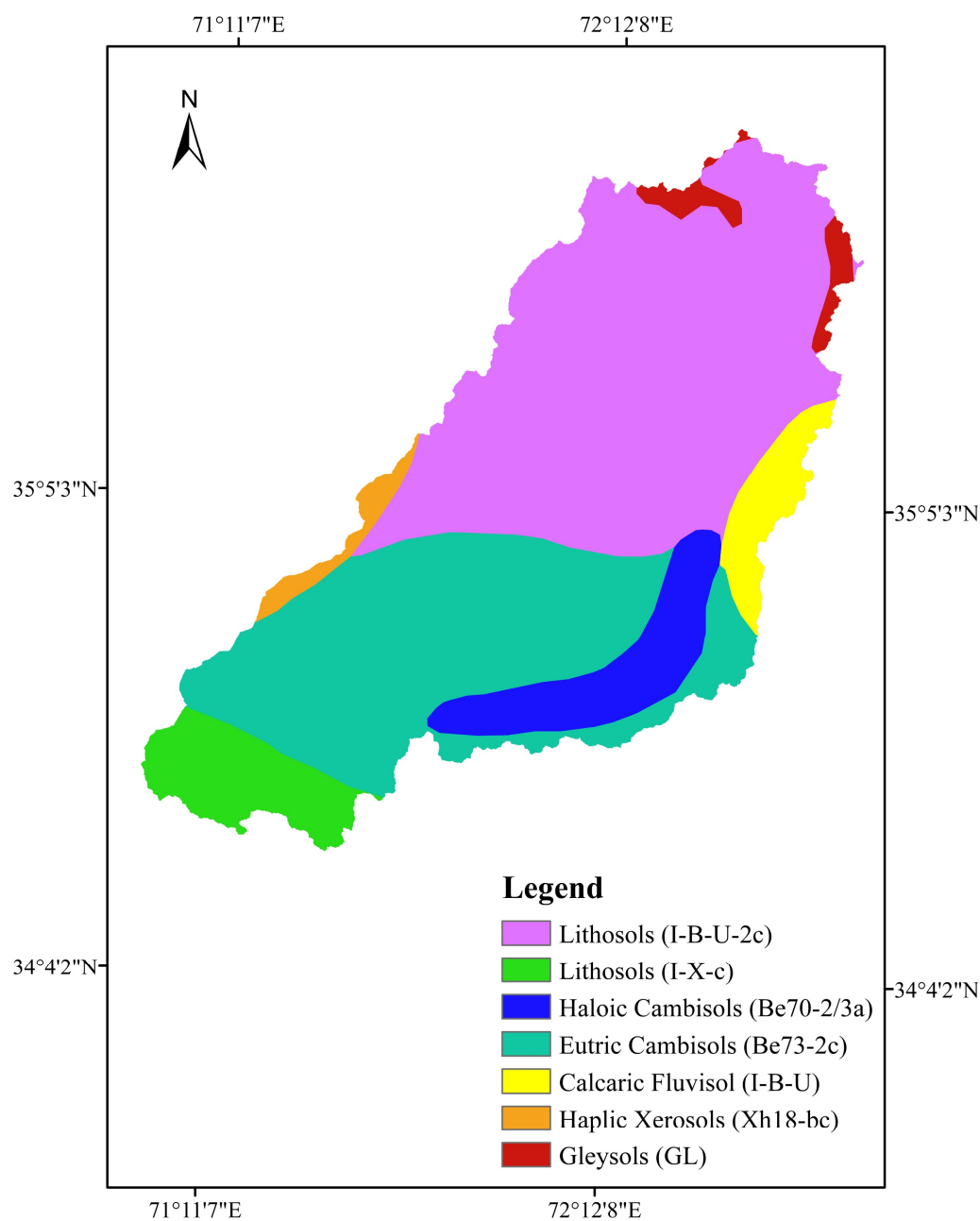


Figure 3. Soil map of the Mohmand Dam catchment area.

2.2.2. GCMs-Based Climate Data

The simulated precipitation (Pr), maximum temperature (Tmax) and minimum temperature (Tmin) data of four GCMs under two SSP scenarios (2 and 5) were downloaded

from the Coupled Model Intercomparison Project phase 6 (CMIP6). Then, outputs of the selected GCMs were downscaled to undertake the analysis on comparable resolutions at the basin scale for the projected temperature and precipitation. The GCMs were selected considering the spatial resolution, vintage, validity and representativeness of the simulations by following the practice of Babur et al. [36]. In the present analysis, out of the four selected GCMs, one better performing GCM was selected based on its ability to simulate the precipitation and temperature during the baseline period (1990–2015). Different statistical downscaling techniques for precipitation and temperature were compared to select the best performing technique for each, which was further used to simulate streamflows in the Mohmand Dam catchment area under climate change conditions. The simulated climatic variables (Tmax, Tmin and Pr) of the selected GCMs were downloaded for medium (SSP2) and high (SSP5) intensities. The descriptions of the GCMs used in the present study are presented in Table 2. In this study, we did not include the low radiative forcing scenario (SSP1). In the current era of industrialization, an immediate drastic decrease in the emission of greenhouse gases is very difficult and, therefore, it is unlikely to meet this mitigation scenario [41]. The medium stabilization forcing scenario (SSP2) and the very high radiative forcing scenario (SSP5) were considered. The projected GCM-based climatic variables under SSP2 and SSP5 were downloaded for the period of 1990–2100, which was then divided into the baseline period (1990–2015) and future time period (2016–2100).

Table 2. Features of GCMs selected for this study.

No.	Model Name	Institute	Nominal Resolution	Release Year
1	MIROC6 (Model for Interdisciplinary Research on Climate, 6th version)	National Institute for Environmental Studies and the Agency for Marine-Earth Science and Technology (MIROC), Japan	250 km	2017
2	MPI-ESM1-2-HR (Max Planck Institute Earth System Model, version 1.2, high resolution)	Max Planck Institute for Meteorology, Germany	100 km	2017
3	ACCESS-CM2 (Australian Community Climate and Earth System Simulator-Coupled Model, version 2)	Australian Community Climate and Earth System Simulator-Coupled Model, Australia	250 km	2016
4	MRI-ESM2-0 (Meteorological Research Institute Earth System Model, version 2.0)	Meteorological Research Institute (MRI) of the Japan Meteorological Agency (JMA)	100 km	2017

2.2.3. Flow Data

The flow data of the Chakdara station and Mohmand Dam site for the time periods 1964 to 2015 and 1999 to 2006, respectively, were obtained from the Water and Power Development Authority (WAPDA), which is a government-owned public utility responsible for managing the country's water and power resources. The data for these sites showed that water levels are highest in the month of July, which is considered the peak flow month. The average flow at the Chakdara and Mohmand Dam stations is 193 and 227.4 cumecs, respectively.

3. Methodology

3.1. Statistical Downscaling

The climate projections of the four different models were downloaded under scenarios SSP2 and SSP5. The CMhyd model was used for bias correction of the GCM-based projected precipitation and temperature estimates at the river basin scale [33,40]. It has been successfully utilized to overcome the bias between GCM-based simulated and gauge-based observed climatic variables in different regions of the world [42]. Anandhi et al., [42] have documented that the CMhyd model is a reliable and robust method to downscale the output of the GCMs for any hydro-climatological studies at the river basin scale. The

CMhyd model provides different statistical downscaling techniques for both precipitation and temperature. In this study, these different approaches were used to downscale the outputs of the GCMs over the future time horizon (2016–2100), under SSP2 and SSP5 conditions. In this context, the time series data of daily projected maximum and minimum temperatures were estimated by integrating the daily precipitation and maximum and minimum temperature during the baseline period (1990–2015) and the projected estimates of the GCMs.

3.2. Description and Setup of the SWAT Model

The soil and water assessment tool (SWAT) is a semi-distributed hydrological model that simulates the impacts of climate change and land management practices on river discharge, water quality and sediment yield [36]. It subdivides a river basin into sub-catchments or hydrological response units (HRUs), and is computationally capable of estimating snow and glacier melt contributions by using a temperature index algorithm (TIA). The SWAT model was used to simulate the river discharge at the Mohmand Dam site under two scenarios: (a) climate change only and (b) land cover and climate change.

The input parameters needed to run the SWAT model were topography, climate, land cover, soil and land use management data. The Mohmand Dam catchment was subdivided into three sub-catchments and 71 HRUs were generated on the basis of land cover and soil type. While, to account for the orographic effects, each sub-catchment was split into 10 elevation bands.

3.3. Calibration and Validation of the SWAT Model

The calibration and validation of the SWAT model were conducted by using the SWAT calibration and uncertainty program (SWAT-CUP), by following Garee et al. [8]. The uncertainty of the model parameters and its performance were checked by using the sequential uncertainty fitting (SUFI-2) in the SWAT-CUP. The best fit values for the sensitive parameters were obtained by running the SWAT-CUP at 10,000 iterations during model calibration. The monthly flow data observed at the Mohmand Dam site during 1999–2002 were considered for the calibration period, while the observed data during 2003–2005 were used for the validation of the simulated results.

Model Performance Evaluation

The performance of the SWAT model was assessed by using the percent bias (PBIAS), the coefficient of determination (R^2) and the Nash–Sutcliffe efficiency (NSE) evaluation indices [43]. The range of R^2 is -1 to 1 , the higher value of R^2 indicate better performance of the simulated results. The values of NSE vary from 0 to 1 , higher values of NSE indicate less error in the simulation and values >0.50 are acceptable [44]. The values of PBAIS ranging between $-15\% < PBIAS < +15$ are acceptable [36]. The mathematical expressions of R^2 and NSE are given below:

$$R^2 = \frac{[\sum(Q_m - \overline{Q_m})(Q_s - \overline{Q_s})]^2}{\sum(Q_m - \overline{Q_m})^2 \sum(Q_s - \overline{Q_s})^2} \quad (1)$$

$$NSE = 1 - \frac{\sum(Q_m - \overline{Q_s})^2}{\sum(Q_m - \overline{Q_m})^2} \quad (2)$$

where, Q_s , Q_m , $\overline{Q_m}$, and $\overline{Q_s}$ stand for simulated discharge, measured discharge, average simulated discharge and average measured discharge respectively.

3.4. Land Cover Scenarios and Validation of Land Cover Prediction

In this study, past and future land cover trends were also discussed by preparing land cover maps of the past years 1995, 2010, 2015, 2018 and 2021 using Landsat imagery and then, the areas were plotted to estimate the change in each class in different years. While

the future land cover maps were prepared for trend analysis and for input into the SWAT model to incorporate future land cover conditions, along with future climate conditions. The land change modeler (LCM) imbedded in the TerrSet was used to simulate future land cover maps. A combined Markov and CA (CA–Markov) model was used in the present study to predict the land cover for 2040, 2070 and 2100. The model was run in two steps using the Markov and CA–Markov module.

3.4.1. Markov Chain Analysis

A tool for predictive change modeling, Markov chain analysis (MCA), is a general macroscopic stochastic modeling procedure. Future developments are predicted using information from the past. If an area has been split into a number of cells, each of which represents a particular form of land use at a given moment, the MCA calculates the chance that a cell will change from one land use class to another within a certain amount of time, based on observed data between time periods. A transition probability is the likelihood of moving from one condition to another. The MCA creates a transition matrix that includes the amount of projected changes in the pixels, as well as the likelihood that each land cover class could shift to another [45]. A Markov transition matrix P can be expressed as follows:

$$\|P_{ij}\| = \begin{vmatrix} P_{1,1} & P_{1,2} & P_{1,N} \\ P_{2,1} & P_{2,2} & P_{2,N} \\ P_{N,1} & P_{N,2} & P_{N,N} \end{vmatrix} \quad (0 \leq P_{ij} \leq 1) \quad (3)$$

where, P_{ij} = the land cover type of the first time period and second time period and P = the probability from land use type 1 to land use type 2. After a certain number of time units, a series of conditional probability images, also known as transitional potential maps, were created. These images indicate the likelihood that each land cover type will be present at each pixel. The reasons for the land cover change are not taken into account in Markov analysis. Another significant issue with Markov analysis is that it is spatially insensitive, providing no sense of geography. Cellular automata are therefore, employed to provide the modeling process with a spatial component.

3.4.2. CA–MARKOV

Cellular automata and a Markov chain-based built-in module named CA–MARKOV from the TerrSet package were used to forecast the future land cover image. A land cover prediction model called CA–MARKOV combined the cellular automata, the Markov chain, multi-criteria and the multi-objective land allocation (MOLA) to add spatial contiguity and information on the anticipated geographical distribution of the transitions into the Markov chain analysis. This is how the algorithm operated: the transition regions file contained the projected amount of land cover change from each existing category to each category in the next time period as determined by a Markov chain analysis of the two previous land use maps. The initial land cover picture was used to start the change simulation (the subsequent land cover image was utilized for the Markov chain analysis). Appropriateness maps or transition potential maps for each land cover were used to determine the inherent suitability of each pixel for each type of land cover [45]. The suitability of the pixels far from the existing areas of that class (as of that iteration) was typically down-weighted by a contiguity filter, favoring suitable contiguous areas instead.

4. Results

4.1. Downscaling of Future Climate Data

The downscaling of the future climate data involved the selection of a GCM and a suitable bias correction technique.

4.1.1. Selection of the GCM

The climate projections of the four different models were downloaded under scenarios SSP2 and SSP5. Out of these four GCMs, the best performing model was selected. The names and other details of the GCMs downloaded and compared are shown in Table 2.

Four main approaches are used in the selection of GCMs depending on the study requirements, such as selection based on: (1) resolution, (2) available data, (3) previous study, and (4) degree of performance indicator.

Performance measures, such as the coefficient of determination (R^2) and the root mean square error (RMSE) between historical GCM data and observed ground data, are used to assess the model's effectiveness. The following tables show the performance of four different CMIP6 GCMs at the Kalam station.

According to the list of climate models for the precipitation, maximum and minimum temperature shown in Tables 3–5, "MPI-ESM1" has comparatively better R^2 , NSE and RMSE values and was selected as the climate model for the assessment of the future climate patterns in the study area. This study assessed climate projections, including precipitation and minimum and maximum temperature that were obtained for the MPI-ESM1 model, under two shared socioeconomic pathways (i.e., SSP2 and SSP5) for a certain duration (2016–2100). These datasets were bias corrected using the climate model data for hydrologic modeling tool (CMhyd).

Table 3. Performance of the GCMs in simulating precipitation.

Model	R^2	NSE	PBIAS	MAE	RMSE
Access-CM2	0.09	−0.81	0.73	71.38	113.56
MIROC6	0.11	−0.48	−0.24	73.71	93.00
MPI-ESM1-2-HR	0.17	0.04	0.22	60.89	86.28
MRI-ESM2	0.10	−0.61	−0.57	68.67	103.96

Table 4. Performance of the GCMs in simulating maximum temperature.

Model	R^2	NSE	PBIAS	MAE	RMSE
Access-CM2	0.16	−1.60	0.25	9.57	11.14
MIROC6	0.20	−1.64	0.39	10.05	19.61
MPI-ESM1-2-HR	0.26	−0.58	0.06	7.62	9.00
MRI-ESM2	0.19	−1.58	0.20	8.55	11.05

Table 5. Performance of the GCMs in simulating minimum temperature.

Model	R^2	NSE	PBIAS	MAE	RMSE
Access-CM2	0.14	−0.93	0.46	12.36	12.40
MIROC6	0.19	−1.84	0.73	16.24	18.77
MPI-ESM1-2-HR	0.23	−0.55	0.26	7.28	9.40
MRI-ESM2	0.18	−0.71	0.31	9.73	11.55

4.1.2. Selection of Bias Correction Techniques

The GCMs provided good results in simulating the observed data on a broader scale, but they still exhibit considerable bias when examined at the basin level [36]. The goal of the bias correction approach was to use a specific correction factor to adjust the model time series variable's mean, variance and/or quintile, so that the corrected model time series closely resembles the observed variable. To select a suitable downscaling technique for the downloaded GCM data, five different precipitation correction techniques (Table 6) and four different temperature correction techniques (Table 6) were compared. All of the techniques were used to correct the precipitation and temperature at the Kalam station and then, their performance was evaluated using time series analysis as shown in Tables 7 and 8.

Table 6. List of bias correction techniques for precipitation and temperature.

Bias Correction for Precipitation	Bias Correction for Temperature
<ul style="list-style-type: none"> • Linear scaling (LS) • Local intensity scaling (LOCI) • Power transformation (PT) • Distribution mapping (DM) • Delta change (DC) 	<ul style="list-style-type: none"> • Linear scaling (LS) • Variance scaling (VS) • Distribution mapping (DM) • Delta change (DC)

Table 7. Comparison of downscaling techniques for precipitation.

Model	Method	R ²	NSE	PBIAS	MAE	RMSE
MPI-ESM1	Raw (model simulated historical)	0.33	0.04	0.22	60.89	86.28
	Delta change	0.68	0.60	0.10	31.72	46.83
	Distribution mapping	0.71	0.73	0.09	28.80	40.02
	Linear scaling	0.65	0.57	0.12	42.61	60.19
	Power transformation	0.75	0.74	0.04	19.42	29.44
	Local intensity scaling	0.66	0.58	0.11	36.27	53.47

Table 8. Comparison of downscaling techniques for maximum and minimum temperature.

Model	Method	R ²	NSE	PBIAS	MAE	RMSE
MPI-ESM1	Maximum temperature					
	Raw (model simulated historical)	0.38	−0.58	0.06	7.62	9.00
	Delta change	0.68	0.36	0.20	3.69	5.72
	Distribution mapping	0.86	0.72	0.02	2.56	3.76
	Linear scaling	0.78	0.56	0.10	2.96	4.73
	Variance scaling	0.75	0.48	0.16	3.32	5.15
	Minimum temperature					
	Raw (model simulated historical)	0.33	−0.55	0.26	7.28	9.40
	Delta change	0.64	0.29	0.18	3.58	6.40
	Distribution mapping	0.88	0.76	0.05	2.11	3.70
	Linear scaling	0.77	0.53	0.14	3.15	5.20
	Variance scaling	0.80	0.64	0.10	2.85	4.56

According to the calculated performance measures, all bias corrections improved the raw GCM simulations. Overall, all bias correction methods were able to correct the monthly mean values for both temperature and precipitation, based on their range of variability and their ability to bring the raw GCM median closer to the observations. The “distribution mapping” performed best for temperature and the “power transformation” for precipitation.

4.2. Probable Changes in the Precipitation and Temperature

After the GCM and downscaling techniques for both precipitation and temperature (max and min) were selected, the projected data were downscaled till the end of the 21st century (2100). Two datasets were created for projected precipitation and temperature, namely the baseline period (1990–2015) and the future scenarios (2016–2100) (e.g., SSP2 and SSP5).

4.2.1. Projection of Mean Maximum Temperature

To assess the future hydrological conditions of Tmax, downscaled future projections of the GCMs were analyzed on an annual and seasonal scale, i.e., winter (December, January and February), spring (March, April and May), summer (June, July and August) and autumn (September, October and November). As per Table 9, the mean maximum

temperature in the catchment increased by 6.9% from 22.42 °C in the baseline period (1990–2015) to 23.98 °C in the future time horizon (2016–2100) under the SSP2 scenario. While, the increase in mean maximum temperature under the worse scenario of SSP5 was 11.1% from 22.4 °C to 24.91 °C.

Table 9. Change in the climatic variables under different climate change scenarios.

Parameters	Statistics	Historical	SSP2	SSP5
Precipitation	mm	1136.05	1255.67	1269.51
	% Change	-	10.5%	11.7%
Max Temperature	°C	22.42	23.98	24.91
	% Change	-	6.9%	11.1%
Min Temperature	°C	7.92	9.20	10.01
	% Change	-	16.1%	26.3%

This change in temperature was analyzed on seasonal basis (winter, spring, summer and autumn). Figure 4 shows the seasonal change in the mean maximum temperature in the Mohmand Dam catchment area. There is an increase in the mean maximum temperature in all the four seasons with highest increase of 12.7% from 12.63 °C in the baseline period to 14.24 °C (Figure 4) under SSP2 and a 21.5% percent increase from 12.63 °C to 15.35 °C (Figure 3) under SSP5 in the winter season. In summer, there was the least increase of 4.1% from 30.69 °C to 31.69 °C under SSP2 and 6.6% from 30.69 °C to 32.73 °C (Figure 4) under SSP5. Similarly, in spring and autumn there was an increase in the maximum temperature under both scenarios (SSP2 and SSP5), with a higher magnitude in SSP5. The increase in spring temperatures was 7.7% and 12.6%, which was an increase up to 24.38 °C and 25.48 °C from 22.63 °C under SSP2 and SSP5 scenarios, respectively. At the end of 21st century (2100), the mean maximum temperature in autumn also increased by 6.8% and 9.8%, as shown by Figure 4.

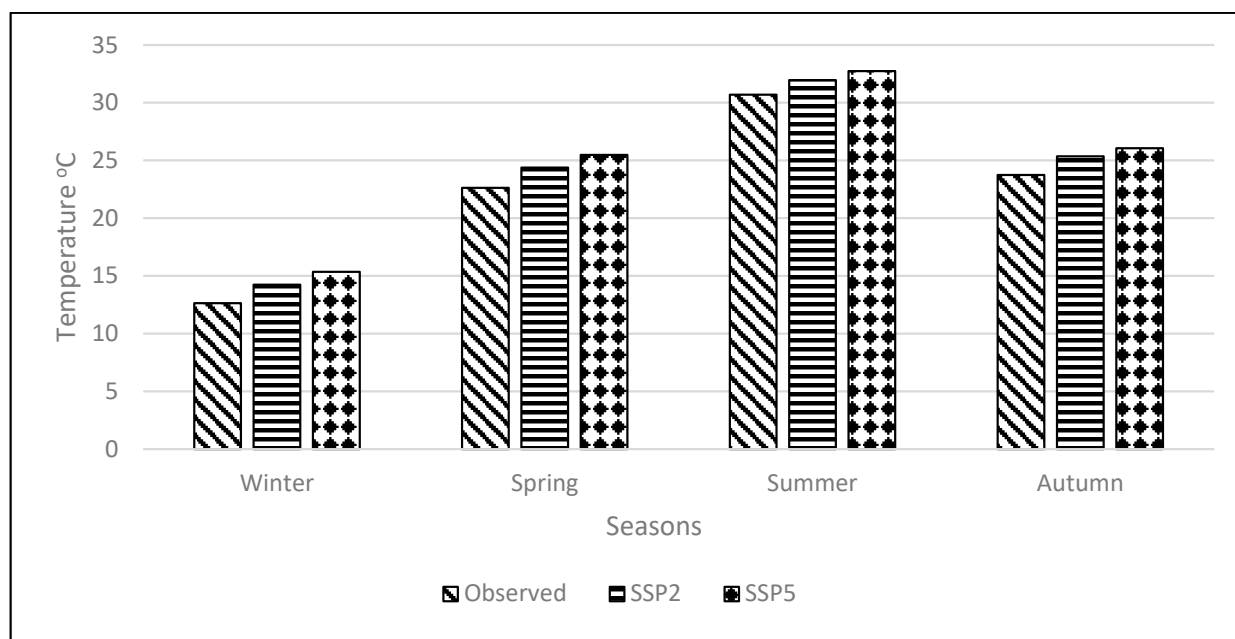


Figure 4. Seasonal change in the maximum temperature in the Mohmand Dam catchment area from 1990 to 2015 for the observed period and 2016 to 2100 for SSP2 and SSP5, respectively.

4.2.2. Projection of Mean Minimum Temperature

To assess the future hydrological conditions of the minimum temperature, downscaled future projections of the GCMs were analyzed at an annual and seasonal scale, i.e., winter

(December, January and February), spring (March, April and May), summer (June, July and August) and autumn (September, October and November). As per Table 9, the mean minimum temperature in the catchment increased by 16.1% from 7.92 °C in the baseline period (1990–2015) to 9.20 °C in the future time horizon (2016–2100) under the SSP2 scenario. While, the increase in the mean minimum temperature under the worse SSP5 scenario was 26.3% from 7.92 °C to 10.01 °C.

This change in temperature was analyzed on a seasonal basis (winter, spring, summer and autumn). Figure 5 shows the seasonal change in the mean minimum temperature in the Mohmand Dam catchment area. There was an increase in the mean minimum temperature for all the four seasons, with the highest increase of 116.6% from -1.35 °C in the baseline period to 0.22 °C (Figure 5) under SSP5 and a 70.4% percent increase from -1.35 °C to -0.40 °C (Figure 5) under SSP2 in the winter season. In summer, there was the least increase of 10.4% from 17.19 °C to 18.97 °C under SSP2 and 17.2% from 17.19 °C to 20.15 °C (Figure 5) under SSP5. Similarly, in spring and autumn there was an increase in the minimum temperature under both scenarios (SSP2 and SSP5), with a higher magnitude in SSP5. The increase in spring temperatures was 13.3% and 20.9%, which was an increase up to 8.89 °C and 9.49 °C from 7.85 °C under SSP2 and SSP5 scenarios, respectively. At the end of 21st century (2100), the mean minimum temperature in autumn also increased by 16.5% and 27.1%, as shown by Figure 5.

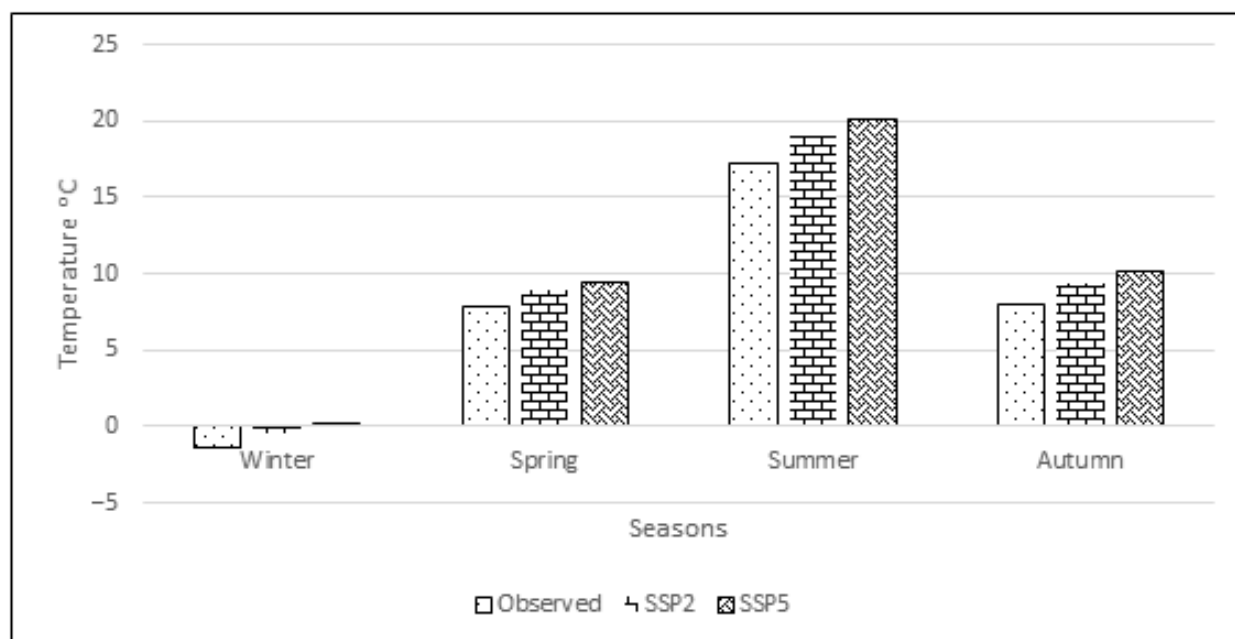


Figure 5. Seasonal change in the minimum temperature in the Mohmand Dam catchment area from 2016 to 2100.

4.2.3. Projection of Precipitation

To assess the future hydrological conditions of precipitation, downscaled future projections of the GCMs were analyzed at an annual and seasonal scale, i.e., winter (December, January and February), spring (March, April and May), summer (June, July and August) and autumn (September, October and November).

As per Table 9, the mean annual precipitation in the catchment increased by 10.5% from 1136.05 mm in the baseline period (1990–2015) to 1255.67 mm in the future time horizon (2016–2100) under the SSP2 scenario. While, the increase in the mean annual precipitation under scenario SSP5 was 11.7% from 1136.05 mm to 1269.51 mm.

This change in precipitation was also analyzed on a seasonal basis (winter, spring, summer and autumn). Figure 6 shows the seasonal change in precipitation in the Mohmand Dam catchment area. There was an increase in the monthly precipitation in all the four

seasons, with the highest increase of 35.2% from 170.2 mm in the baseline period to 230.1 mm (Figure 6) under SSP5 and a 22.4% percent increase from 170.2 mm to 230.15 mm (Figure 6) under SSP2 in the autumn season. In spring, there was the least increase of 0.7% from 408 mm to 410.8 mm under SSP2 and 5.2% from 408 mm to 429.3 mm (Figure 6) under SSP5. Similarly, in winter and summer there was an increase in precipitation under both scenarios SSP2 and SSP5. The increase in winter precipitation was 6.2% and 0.4%, which was an increase up to 304.2 mm and 321.9 mm from 303 mm under SSP2 and SSP5 scenarios, respectively. At the end of 21st century (2100), the precipitation in summer also increased by 0.7% and 5.2%, as shown in Figure 6.

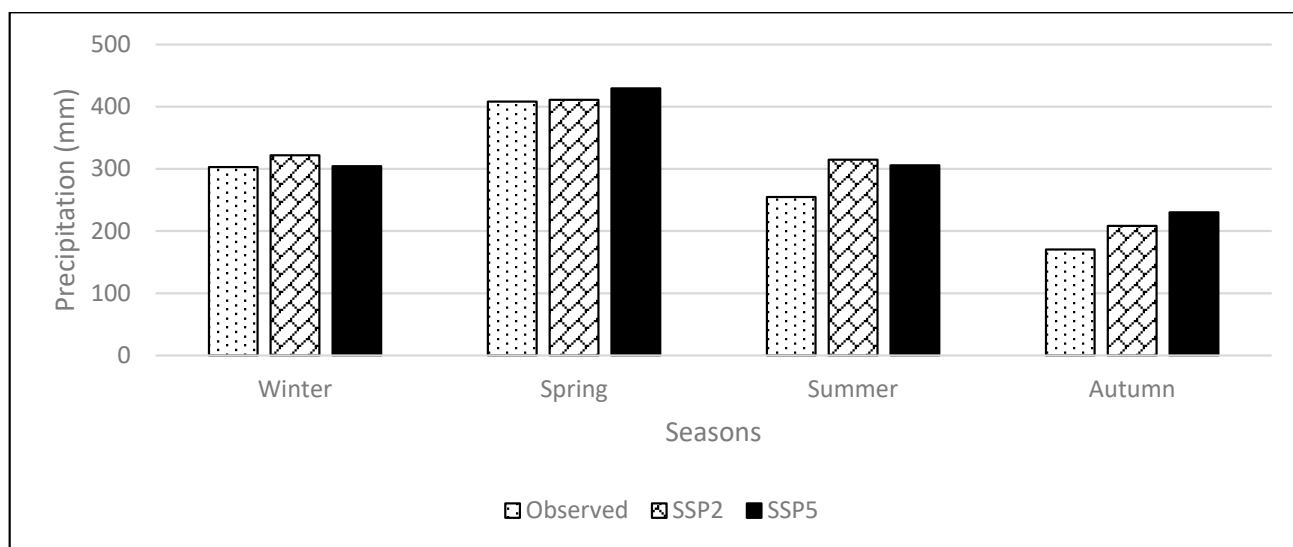


Figure 6. Seasonal change in precipitation in the Mohmand Dam catchment area from 2016 to 2100.

This increase in precipitation may be due to climate change, which causes warmer air due to higher temperatures, as anticipated by both climate change scenarios (SSP2 and SSP5), thus the air can hold more moisture. As the Earth's temperature increases, the atmosphere can hold more moisture. This means that more water evaporates from the oceans, and when it falls as precipitation, it can result in heavier rain or snowfall events. Secondly, this increase in precipitation can be attributed to changes in land cover, such as deforestation or urbanization, which can alter the hydrological cycle, leading to changes in precipitation patterns. For example, deforestation can lead to reduced evapotranspiration, which can lead to less rainfall in some regions.

4.3. Land Cover Change Trends

The supervised image classification of the mosaicked Landsat for 1995, 2010, 2013, 2015, 2018 and 2021 was conducted by using the image classification tool in ArcGIS. Classified maps of the study area are given below in Figure 7. The images were classified into six classes, i.e., built-up area, vegetation, water body, snow cover, forest and barren land. The results indicated that the built-up area, vegetation and water body areas in the catchment of the Mohmand Dam increased by 2.6%, 9.5% and 8.6% from 1995 to 2021. While, other land cover classes like forest, barren land and snow cover decreased by the magnitude of 6.2%, 7.7% and 6.8%, respectively. The change in land cover classes is depicted in Figure 8.

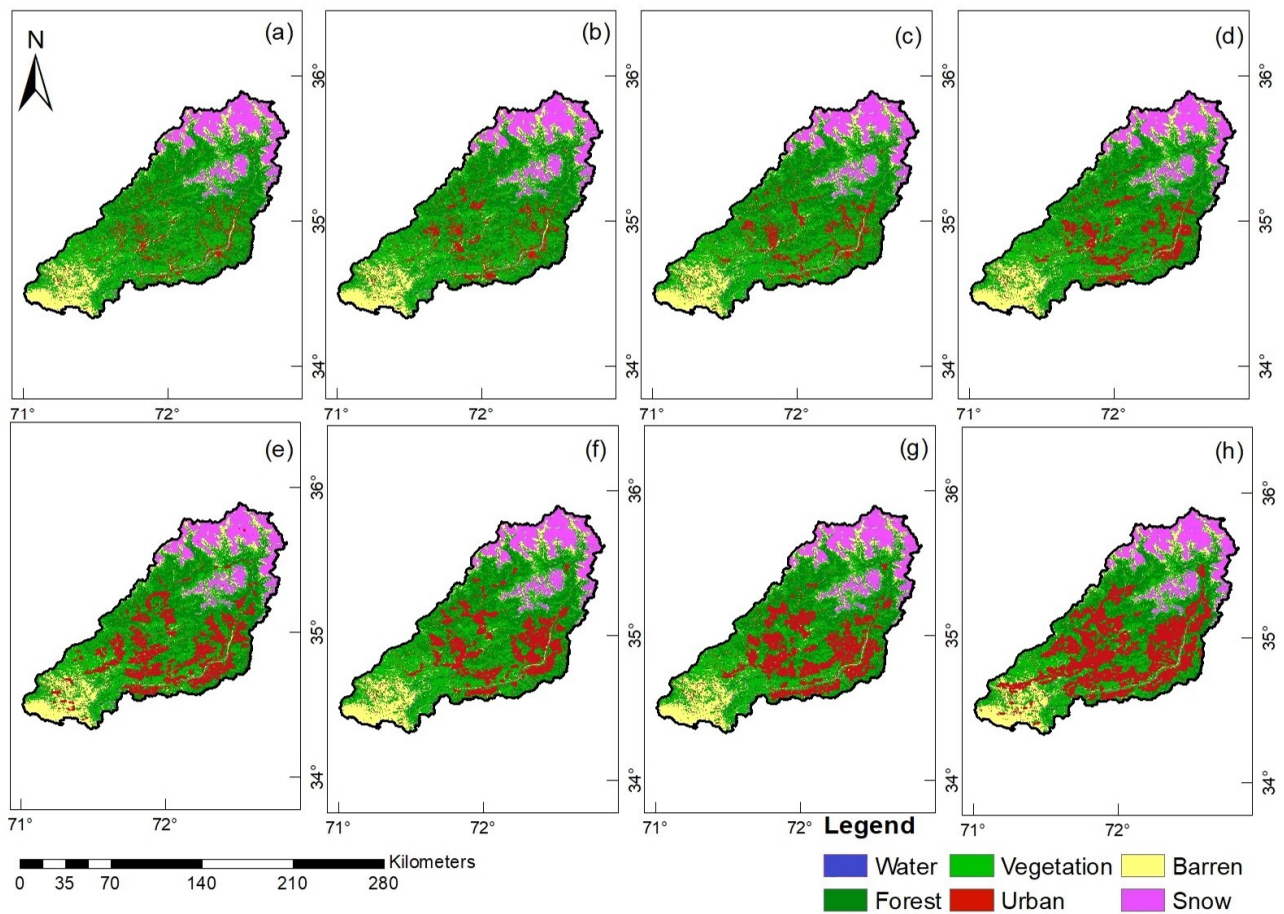


Figure 7. Classified maps for different years: (a) 1995, (b) 2010, (c) 2015, (d) 2018, (e) 2021, (f) 2030, (g) 2060, and (h) 2100.

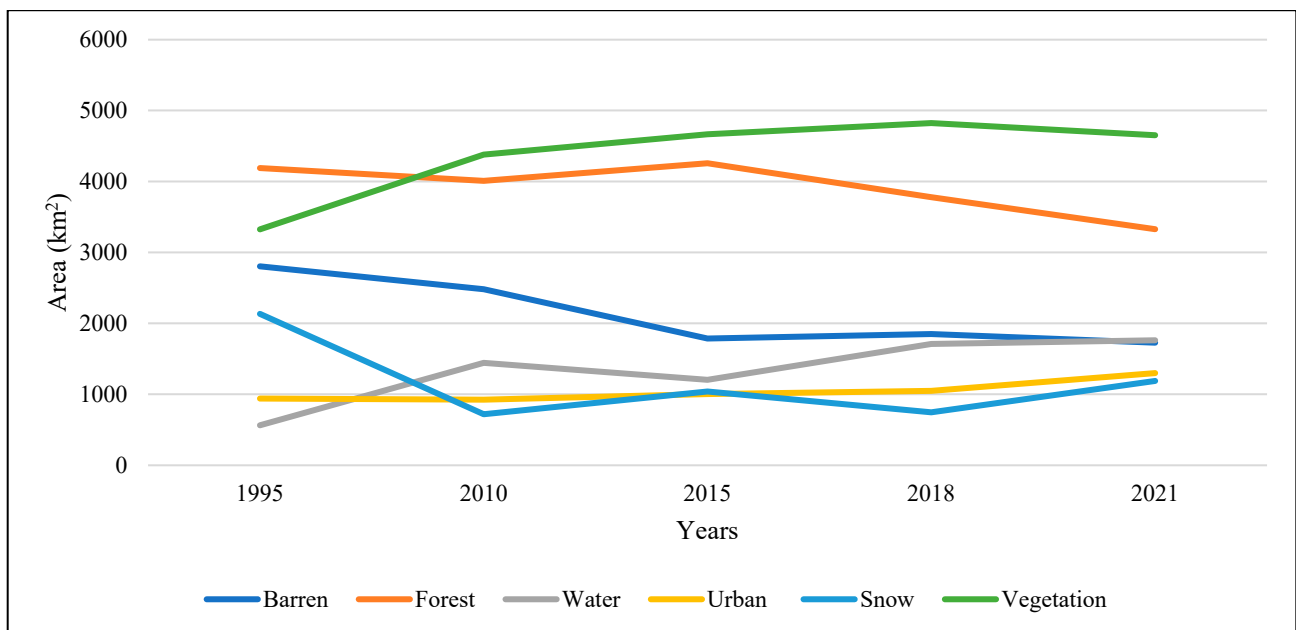


Figure 8. Trends in land cover change from 1995 to 2021.

Future Land Cover Maps

As the landcover map was one of the inputs in the SWAT model, so as to incorporate future land cover conditions into the SWAT Model, landcover maps for 2030, 2060 and 2100 were prepared using the land change modeler imbedded in TerrSet. TerrSet is a geospatial monitoring and modeling system of tools for the analysis of image time series, developed in 1987 by Prof. J. Ronald of Clark University. It uses the Cellular Automata-Markov Chain Model (CA-MCM) for the simulation of future land cover.

Projected land cover maps on the study area are given in Figure 7. According to the results of the study, the built-up area and water body areas in the catchment of the Mohmand Dam increased by 9.5% and 4.6% from 2015 to 2100, respectively. While, other landcover classes like forest, vegetation, barren land and snow cover decreased by a magnitude of 6.8%, 1.4%, 5.3% and 0.6%, respectively. This change in land cover classes is depicted in Figure 9.

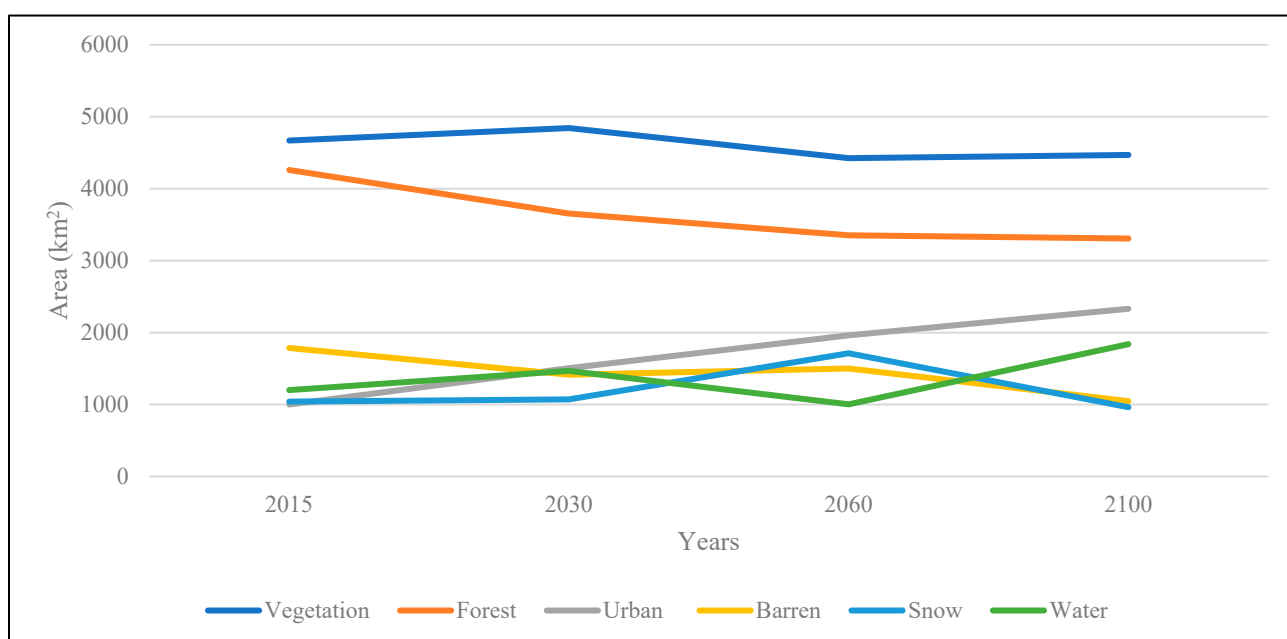


Figure 9. Trends in land cover change from 2015 to 2100.

4.4. Calibration and Validation of the SWAT Model

For the calibration of the SWAT model, it was essential to adjust the sensitive parameters, including parameters for snow, soil, groundwater recharge and evapotranspiration. In this study, 22 parameters that influenced the total simulated outflow at the outlet of the Swat River basin were found to be sensitive (Table 10). These modeling parameters were selected by considering their significant influence on the snow/glacier melt runoff, ET and groundwater recharge, in addition to the available literature on the application of the SWAT model to glaciated watersheds [10,25,46]. During the winter months, the majority of the precipitation is in the form of snow, especially in northern regions of the basin. The Swat River at the Chakdara gauge has a mean annual discharge of 243 m³/s, according to river flow data from a 54-year period (1961–2014). The month of peak discharge is known to be July. The values of R2 and NSE for the calibration and validation period are given in Table 11. The monthly calibration and validation for the Swat River is shown in Figures 10 and 11, respectively.

Table 10. Descriptions of the sensitive parameters with their adopted values.

Parameter Name	Fitted Value	Min Value	Max Value
A_REVAPMN.gw	200.225494	196	205
V_ESCO.hru	0.62635	0.4	0.7
A_HRU_SLP.hru	0.00882	0	0.12
A_SLSUBBSN.hru	58.1325	55	90
V_CH_K2.rte	138.827499	130	145
V_SMFMN.bsn	0.08125	0	6.5
A_SURLAG.bsn	12.341	11	17
V_CN2.mgt	89.525002	70	92
V_CH_N2.rte	0.09975	0	0.1
V_SFTMP.bsn	4.971110	4	5
R_OV_N.hru	0.09255	0	0.1
R_SOL_BD(..).sol	1.2704	0.9	2.5
R_SOL_K(..).sol	0.172985	0.16	0.23
V_TLAPS.sub	−0.7918	−1	0.2
V_TIMP.bsn	0.02755	0	0.1
V_PLAPS.sub	44.4375	25	50
V_GW_DELAY.gw	286.875	270	320
V_SMFMX.bsn	0.37575	0	4.5
V_GWQMN.gw	3990.625	3400	4150
R_SOL_AWC(..).sol	0.122825	0.11	0.3
R_CANMX.hru	47.57	30	50
V_CH_N1.sub	1.49275	1	3.7

Table 11. Statistical summary of the monthly calibration and validation of the SWAT model.

	Calibration	Validation
R2	0.81	0.78
NSE	0.79	0.74
PBIAS	−10.6	11

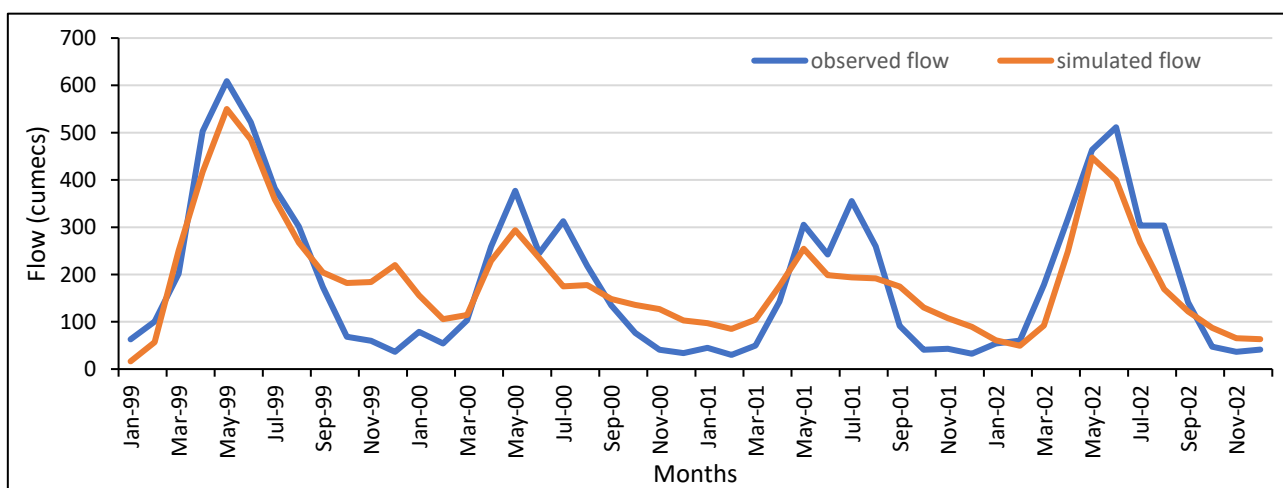


Figure 10. Comparison between the observed and simulated monthly flows (cumeecs) in the calibration period (1999–2002).

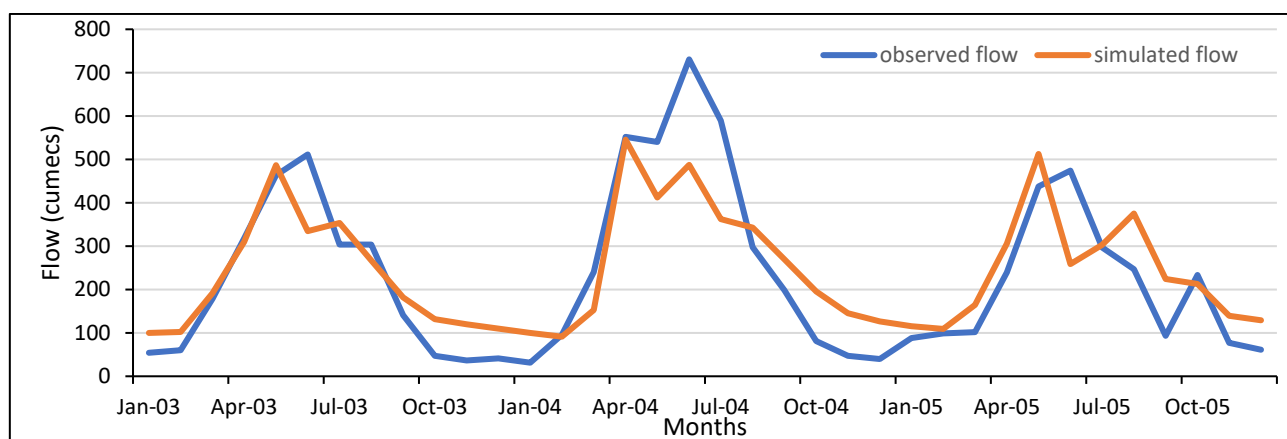


Figure 11. Comparison of monthly observed and simulated flows (cumecs) in the validation period (2003–2005).

4.5. Impact of Projected Climate on Flows

After calibration and validation of the model, this setup was applied for the future prediction of flows on an annual basis for the years 2016 to 2100. There are two scenarios for which the future flows were assessed.

Scenario A: In the first scenario, the current land cover conditions and future climate were used to predict the flows due to expected climate change.

Scenario B: In the second scenario, the future land cover and future climate conditions were used to assess the combined impact of future land cover and climate change.

4.5.1. Scenario A: Climate Change Only

The calibrated model was used for the prediction of flows, based on the climate change data for the next three decades. The precipitation increased by 10.53% and 11.74% under SSP2 and SSP5, while the maximum temperature increased by 6.95% and 11.07%, respectively. Similarly, the minimum temperature increased by 16.09% to 8.82% under SSP2 and SSP5, respectively. This change in precipitation and temperature when forced into the calibrated SWAT model under constant land cover conditions (current) predicted that the flows are expected to increase from 227.4 cumecs in the baseline period (1999–2015) to 258.72 cumecs (an increase of 13.77%) and 264.53 cumecs (an increase of 16.29%) in future time horizon (2016–2100) under SSP2 and SSP5, respectively. Figures 12 and 13 show the comparison between the past and predicted flows due to climate change.

Figure 14 compares the mean monthly flows for the baseline period (1999–2015) with those for the future time horizon under the SSP2 and SSP5 scenarios, in order to examine the temporal changes in the mean monthly flows in the Mohmand Dam catchment area. In general, both SSPs predicted an increase in the flow during the low flow months and a drop in the mean monthly flow during the high flow months. The average seasonal flow was predicted to rise throughout the year, while decreasing in the summer. Both SSPs anticipate an increase in the peak flows (July to June) at the dam site (2 and 5). This might be connected to the westerlies circulation pattern. The increase in winter precipitation may be the cause of an increase in the winter flows. The reduction in monsoon precipitation in this area may be one factor in the decline in summer flows. The months with the highest and lowest flows under both SSPs were June and January, respectively.

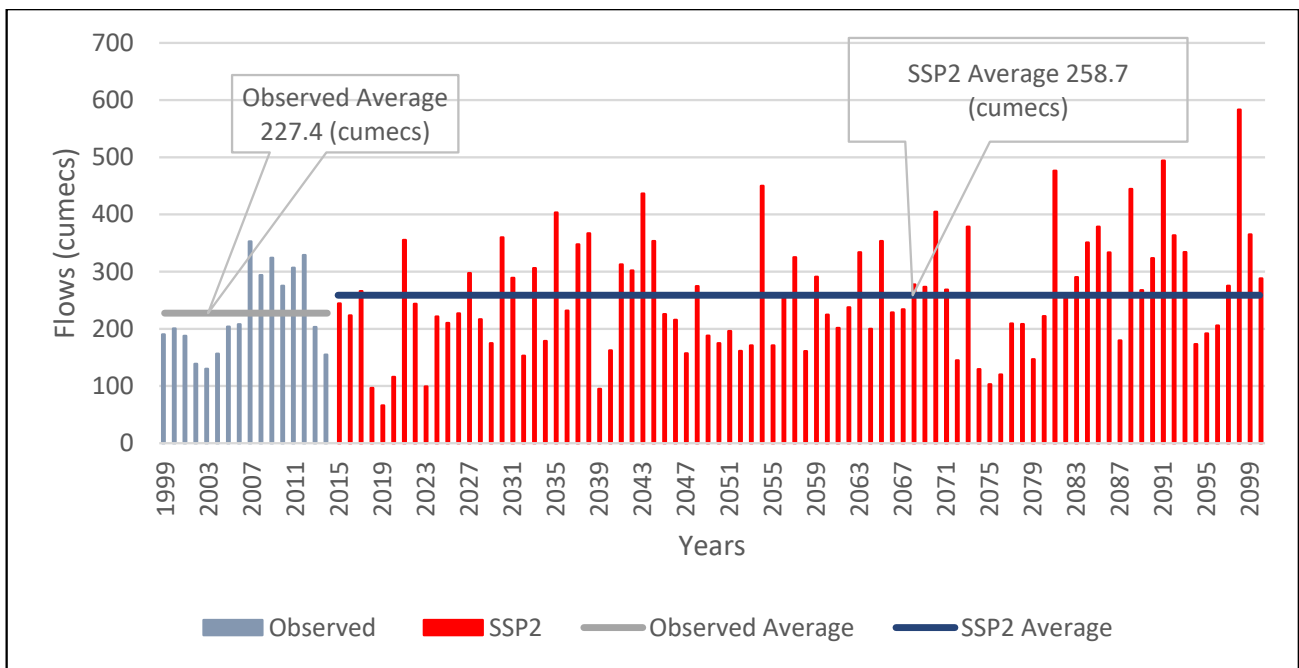


Figure 12. Comparison between the past and predicted flows under SSP2, according to the current land cover and future climate.

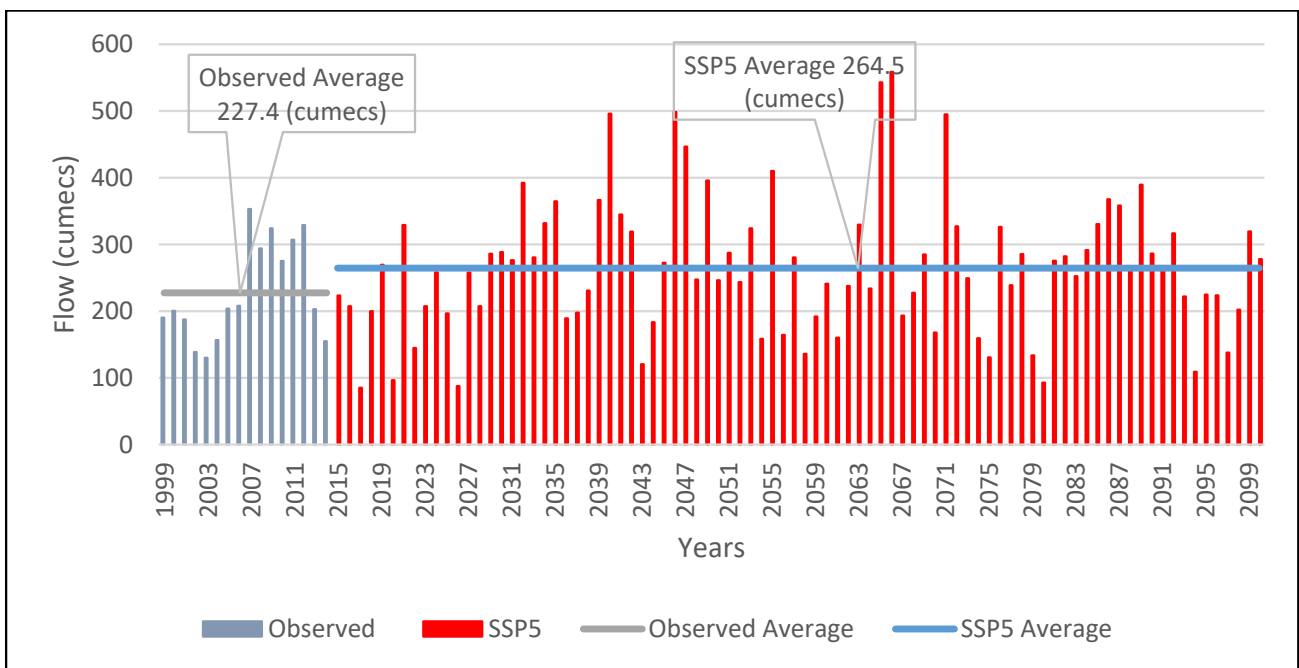


Figure 13. Comparison between the past and predicted flows under SSP5, according to the current land cover and future climate.

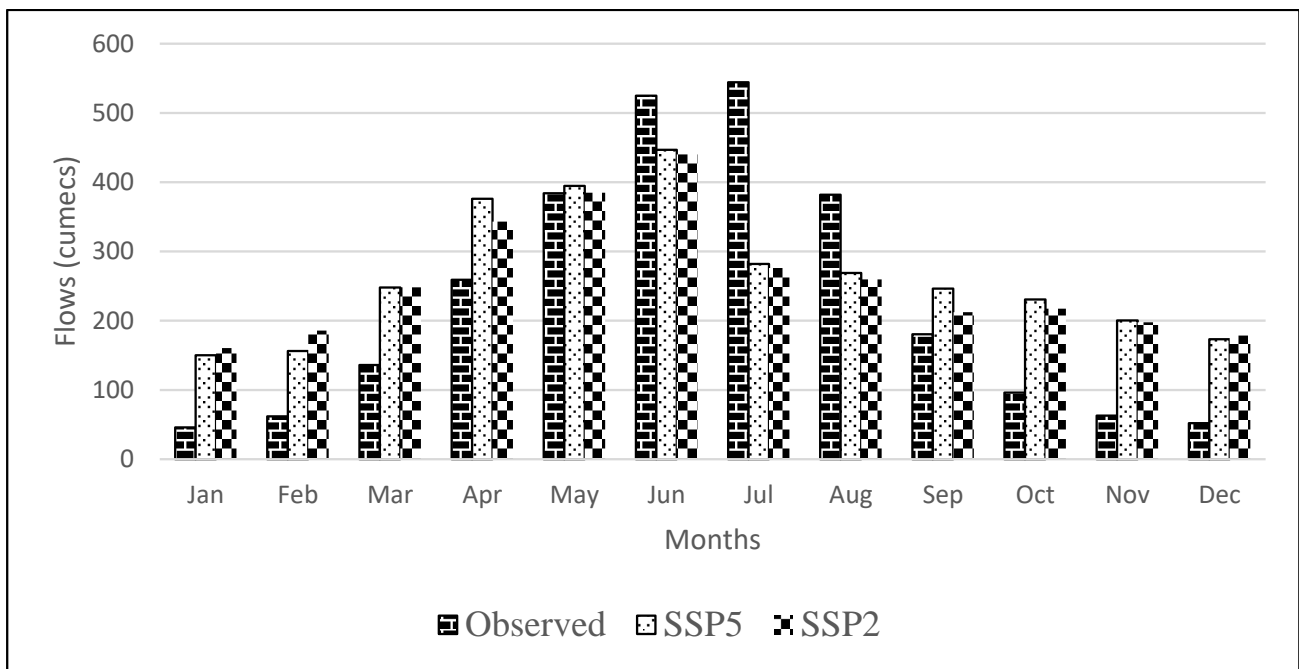


Figure 14. Mean monthly flows at the dam site under current land cover and future climate conditions.

4.5.2. Scenario B: Climate and Land Cover Change

After the prediction of the flows for climate change only, the calibrated model was used for the prediction of flows based on the climate and land cover change.

The land cover trends indicated that the built-up area and water body areas in the catchment of the Mohmand Dam increased by 9.5% and 4.6% from 2016 to 2100. While, other land cover classes like forest, vegetation, barren land and snow cover decreased by the magnitude of 6.8%, 1.4%, 5.3% and 0.6%, respectively. On the other hand, precipitation increased by 10.53% and 11.74% under SSP2 and SSP5, respectively, while the maximum temperature increased by 6.95% and 11.07%. Similarly, the minimum temperature is increased by 16.09% to 8.82% under SSP2 and SSP5, respectively. This change in land cover and climate when forced into the calibrated SWAT model under constant land cover conditions (current) predicted that the flows are expected to increase from 227.4 cumecs in the baseline period (1999–2015) to 289.82 cumecs (an increase of 27.4%) and 306.61 cumecs (an increase of 34.8%) in the future time horizon (2016–2100) under SSP2 and SSP5, respectively. Figures 15 and 16 show the comparisons between the past and predicted flows due to climate and land cover change.

This increase in flow under both SSP scenarios could be attributed to increased precipitation as mentioned earlier, climate change is causing an increase in precipitation in many regions of the world. When precipitation falls on land, it can either evaporate, be taken up by plants, or flow into rivers and streams as runoff. With more precipitation, there is more runoff, which can increase streamflow. Moreover, earlier snowmelt could be another reason for this increase in flows as climate change is causing warmer temperatures, which can cause snow to melt earlier in the year. This can result in increased streamflow during the spring and summer months, when snowmelt is typically the primary source of water for rivers and streams. Hence, under both scenarios precipitation and temperature were increased and this increase ultimately affected the flows.

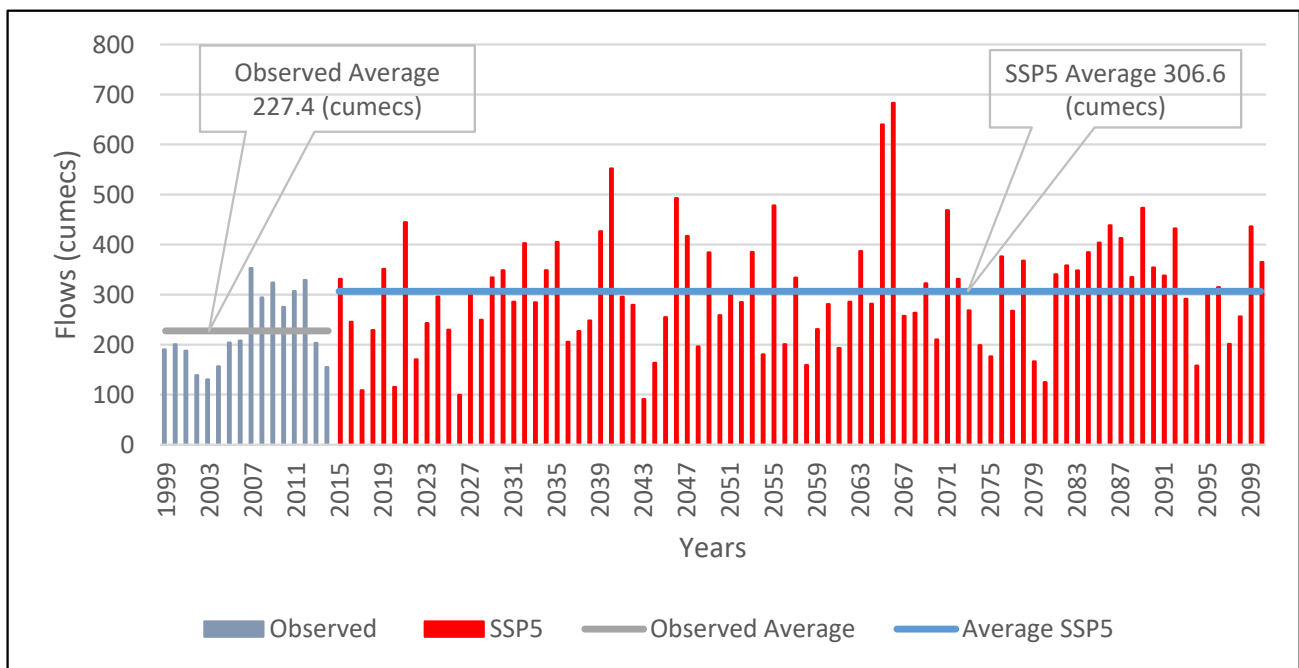


Figure 15. Comparison between past and predicted flows under SSP5, according to future land cover and climate change.

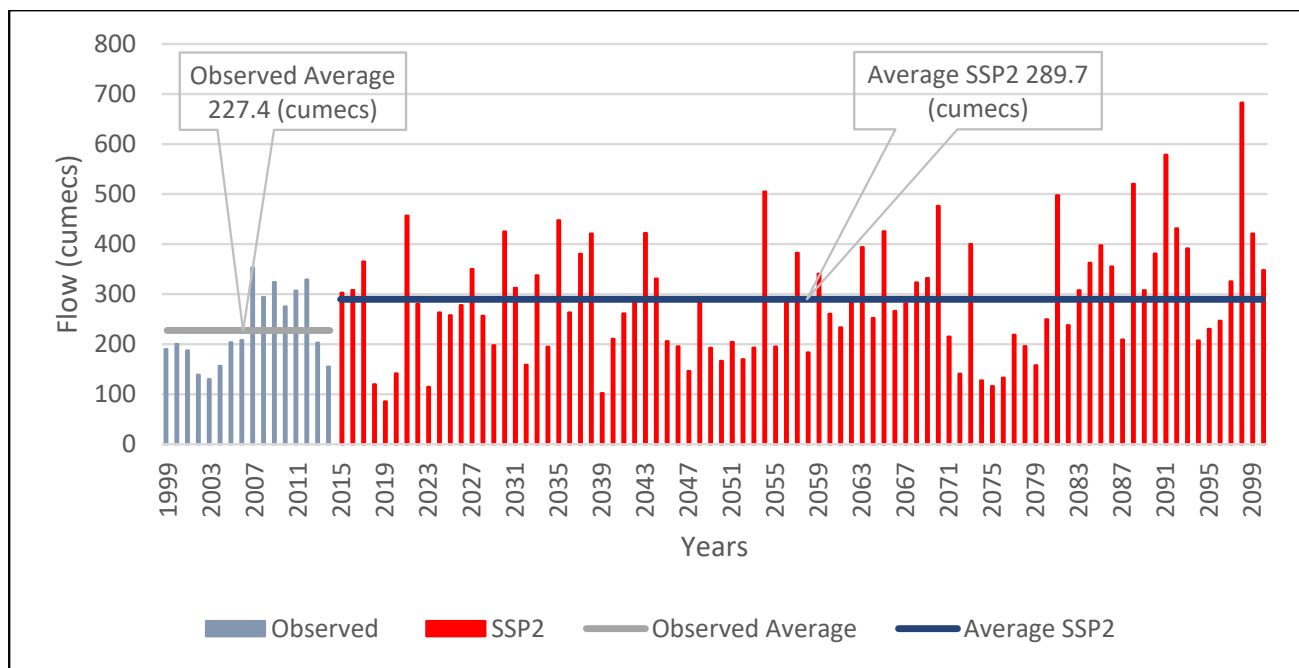


Figure 16. Comparison between past and predicted flows under SSP2, according to future land cover and climate change.

5. Discussion

This study evaluated the effects of projected land cover and climate change on the flows of the Mohmand Dam catchment area, using CMIP6 global climate models (GCMs) to develop a calibrated soil and water assessment tool (SWAT) hydrological model. The findings from the analysis of the GCM outputs (MPI-ESM1-2-HR) pointed to a persistent warming on annual and seasonal scales of the catchment area of the Mohmand Dam in the 21st century, which is consistent with those in the neighboring south Asian regions of the

Tibetan Plateau [47,48] and Himalaya [8,36,49]. Increased concentrations of greenhouse gases in the local environment could be a contributing factor to the noticeably higher temperatures at HKH mountains [12,50]. The average amount of precipitation each year is expected to rise in the future (2016–2100). The headwaters of the Yellow River basin were also observed to increase between the years 2015 and 2100 [43]. The GCM predicts that precipitation will tend to increase during the future time horizon, with summer and autumn observing the greatest increases. These findings are in contradiction with those for Malaysia's Kelantan River basin and the upper Cruz River basin [46,51]. Additionally, Ozturk et al. [52] discovered a paradox in the form of a tendency for summer precipitation to decrease in areas where the westerlies are dominant (Afghanistan and Iran). The seasonal precipitation patterns of the study area, though, are consistent with those in the Himalayan and Karakoram ranges. The Jhelum River basin, which is located in the Himalayan range, has a persistently increasing tendency toward annual and seasonal precipitation, according to Babur et al. [36]. In the Hunza River basin, which is located in the Karakoram range, Garee et al. [8] predicted an increasing tendency for precipitation in the inter-annual and seasonal precipitation. The westerlies circulation system, which is predominant in the Hindukush range, may be responsible for these agreements in the results [12,14,26]. The rising concentration of anthropogenic absorbing aerosols in the south Asian atmosphere is another possible explanation for these similarities in precipitation behavior [53–55].

The yearly average flow over the future time horizons under both SSPs (SSP2 and SSP5) is increasing, according to the analysis of the simulated flows obtained from the SWAT model. The anticipated increases in yearly precipitation and warming temperature may be related to an increase in the flow in the future. The Indus River flow has been predicted to increase by Immerzeel et al. [56] as well. In addition, it is predicted that the peak flows may move up by one month (from July to June), primarily as a result of the considerable rise in precipitation over the winter and spring seasons. However, Babur et al. [36] discovered a delay in the peak flow of the Jhelum River, which typically occurs between July and August. The disagreement in the findings may be caused by the various anticipated trends for winter and summer precipitation at the Hindukush and Himalayan Mountains.

6. Conclusions

In the present study, the impacts of climate and land cover change on the Swat River flows were assessed by using the SWAT model under two scenarios, namely climate change only and climate and land cover change in future time horizon (2016–2100) under two SSPs (2 and 5). For the projection of climate change, the outputs of four GCMs were compared and the best performing GCM was selected; then, five statistical downscaling techniques for precipitation and four techniques for temperature were compared and the best performing technique for each aspect was selected to be used for the study area. While, for future land cover projection the land change modeler imbedded in TerrSet was used. The SWAT hydrological model was calibrated and validated for the 1999–2002 and 2003–2005 periods, respectively. The results of the evaluation indices (PBIAS, R2 and NSE) for both the calibration and validation periods showed that the hydrological model was well calibrated and was reliable to be used for the projection of potential impacts of climate and land cover change on the Swat River flows. After analysis of the streamflows in the Swat River at the Mohmand Dam site under the projected future climate and land cover conditions, the following conclusions have been drawn:

- Compared to the baseline period (1990–2015), the annual maximum, minimum and mean temperature and precipitation increased consistently in the Mohmand Dam catchment in the future time horizon (2016–2100). The increased precipitation leads to increased streamflows in the future;
- The average daily streamflow at the Mohmand Dam site increased from 227.4 cumecs (1999–2015) to 258.7 cumecs under SSP2 and to 264.5 cumecs under SSP5 using the present land cover conditions;

- Under the future land cover change scenario, the flow increased from 227.4 cumecs (1999–2015) to 289.8 cumecs and 306.6 cumecs under SSP2 and SSP5, respectively;
- The land cover and climate change scenarios results revealed that the overall mean monthly flows will increase by 27.4% and 34.8% under both SSPs, whereas the mean monthly flows in June, July and August will decrease (Figure 14), while the flows for November, December and January will increase under both SSPs (Figure 14); and
- The peak flow in the Mohmand Dam catchment is anticipated to advance by a month, i.e., from July to June in future scenarios of land cover and climate change conditions (Figure 14).

The present study focuses on the future change in precipitation and temperature (maximum and minimum) and their impacts on the Swat River flows. The findings of this study might be useful for formulating regional development and adaptation strategies, as well as for the sustainable planning and management of water resource projects, including hydropower and irrigation schemes.

Author Contributions: All authors were involved in the intellectual elements of this paper. M.U.M., N.M.K., X.C. and M.N.A. designed the research. M.U.M. and S.H. conducted the research and wrote the manuscript. A.G., M.I., Z.A. and T.L. helped in the data arrangement and analysis. All authors have read and agreed to the published version of the manuscript.

Funding: This study was supported by the National Natural Science Foundation of China (Grant No. 42230708), the Research Fund for International Scientists of the National Natural Science Foundation of China (Grant No. 42150410393), the Strategic Priority Research Program of the Chinese Academy of Sciences, the Pan-Third Pole Environment Study for a Green Silk Road (Grant No. XDA20060303), the Xinjiang Scientific Expedition Program (Grant No. 2021XJKK1044), the K.C. Wong Education Foundation (Grant No. GJTD-2020-14), and the CAS Research Center for Ecology and Environment of Central Asia (Grant No. Y934031).

Data Availability Statement: The data are not publicly available due to further research.

Conflicts of Interest: The authors declare no conflict of interest.

References

1. Arheimer, B.; Donnelly, C.; Lindström, G. Regulation of snow-fed rivers affects flow regimes more than climate change. *Nat. Commun.* **2017**, *8*, 62. [[CrossRef](#)]
2. Bolch, T. Asian glaciers are a reliable water source. *Nature* **2017**, *545*, 161–162. [[CrossRef](#)] [[PubMed](#)]
3. Deng, H.; Chen, Y.; Wang, H.; Zhang, S. Climate change with elevation and its potential impact on water resources in the Tianshan Mountains, Central Asia. *Glob. Planet. Chang.* **2015**, *135*, 28–37. [[CrossRef](#)]
4. Lutz, A.; Immerzeel, W.; Shrestha, A.B.; Bierkens, M.F. Consistent increase in High Asia’s runoff due to increasing glacier melt and precipitation. *Nat. Clim. Chang.* **2014**, *4*, 587–592. [[CrossRef](#)]
5. Sharma, C.S.; Panda, S.N.; Pradhan, R.P.; Singh, A.; Kawamura, A. Precipitation and temperature changes in eastern India by multiple trend detection methods. *Atmos. Res.* **2016**, *180*, 211–225. [[CrossRef](#)]
6. Haider, H.; Zaman, M.; Liu, S.; Saifullah, M.; Usman, M.; Chauhdary, J.; Anjum, M.; Waseem, M. Appraisal of Climate Change and its Impact on Water Resources of Pakistan: A Case Study of Mangla Watershed. *Atmosphere* **2020**, *11*, 1071. [[CrossRef](#)]
7. Yao, T.D.; Thompson, L.; Yang, W.; Yu, W.S.; Gao, Y.; Guo, X.J.; Yang, X.X.; Duan, K.Q.; Zhao, H.B.; Xu, B.Q.; et al. Different glacier status with atmospheric circulations in Tibetan Plateau and surroundings. *Nat. Clim. Chang.* **2012**, *2*, 663–667. [[CrossRef](#)]
8. Garee, K.; Chen, X.; Bao, A.; Wang, Y.; Meng, F. Hydrological Modeling of the Upper Indus Basin: A Case Study from a High-Altitude Glacierized Catchment Hunza. *Water* **2017**, *9*, 17. [[CrossRef](#)]
9. Cheema, M.; Immerzeel, W.; Bastiaanssen, W. Spatial Quantification of Groundwater Abstraction in the Irrigated Indus Basin. *Groundwater* **2013**, *52*, 25–36. [[CrossRef](#)]
10. Khan, A.; Naz, B.S.; Bowling, L.C. Separating snow, clean and debris covered ice in the Upper Indus Basin, Hindukush-Karakoram-Himalayas, using Landsat images between 1998 and 2002. *J. Hydrol.* **2015**, *521*, 46–64. [[CrossRef](#)]
11. Ali, S.; Eum, H.-I.; Cho, J.; Dan, L.; Khan, F.; Dairaku, K.; Shrestha, M.L.; Hwang, S.; Nasim, W.; Khan, I.A.; et al. Assessment of climate extremes in future projections downscaled by multiple statistical downscaling methods over Pakistan. *Atmos. Res.* **2019**, *222*, 114–133. [[CrossRef](#)]
12. Anjum, M.N.; Ding, Y.; Shangguan, D.; Ahmad, I.; Ijaz, M.W.; Farid, H.U.; Yagoub, Y.E.; Zaman, M.; Adnan, M. Performance evaluation of latest integrated multi-satellite retrievals for Global Precipitation Measurement (IMERG) over the northern highlands of Pakistan. *Atmos. Res.* **2018**, *205*, 134–146. [[CrossRef](#)]

13. Tahir, A.A.; Adamowski, J.F.; Chevallier, P.; Haq, A.U.; Terzago, S. Comparative assessment of spatiotemporal snow cover changes and hydrological behavior of the Gilgit, Astore and Hunza River basins (Hindukush–Karakoram–Himalaya region, Pakistan). *Meteorol. Atmos. Phys.* **2016**, *128*, 793–811. [[CrossRef](#)]
14. Dahri, Z.H.; Ludwig, F.; Moors, E.; Ahmad, B.; Khan, A.; Kabat, P. An appraisal of precipitation distribution in the high-altitude catchments of the Indus basin. *Sci. Total. Environ.* **2016**, *548*, 289–306. [[CrossRef](#)] [[PubMed](#)]
15. Filippi, L.; Palazzi, E.; von Hardenberg, J.; Provenzale, A. Multidecadal Variations in the Relationship between the NAO and Winter Precipitation in the Hindu Kush–Karakoram. *J. Clim.* **2014**, *27*, 7890–7902. [[CrossRef](#)]
16. Hasson, S.U.; Böhner, J.; Lucarini, V. Prevailing climatic trends and runoff response from Hindukush–Karakoram–Himalaya, upper Indus Basin. *Earth Syst. Dyn.* **2017**, *8*, 337–355. [[CrossRef](#)]
17. Archer, D.R.; Forsythe, N.; Fowler, H.J.; Shah, S.M. Sustainability of water resources management in the Indus Basin under changing climatic and socio economic conditions. *Hydrol. Earth Syst. Sci.* **2010**, *14*, 1669–1680. [[CrossRef](#)]
18. Ahmed, N.; Wang, G.; Booij, M.J.; Xiangyang, S.; Hussain, F.; Nabi, G. Separation of the Impact of Landuse/Landcover Change and Climate Change on Runoff in the Upstream Area of the Yangtze River, China. *Water Resour. Manag.* **2022**, *36*, 181–201. [[CrossRef](#)]
19. Chernos, M.; MacDonald, R.J.; Straker, J.; Green, K.; Craig, J.R. Simulating the cumulative effects of potential open-pit mining and climate change on streamflow and water quality in a mountainous watershed. *Sci. Total. Environ.* **2022**, *806*, 150394. [[CrossRef](#)]
20. Philip, E.; Rudra, R.P.; Goel, P.K.; Ahmed, S.I. Investigation of the Long-Term Trends in the Streamflow Due to Climate Change and Urbanization for a Great Lakes Watershed. *Atmosphere* **2022**, *13*, 225. [[CrossRef](#)]
21. Ahmed, N.; Wang, G.; Lü, H.; Booij, M.J.; Marhaento, H.; Prodhon, F.A.; Ali, S.; Imran, M.A. Attribution of Changes in Streamflow to Climate Change and Land Cover Change in Yangtze River Source Region, China. *Water* **2022**, *14*, 259. [[CrossRef](#)]
22. Shokouhifar, Y.; Lotfirad, M.; Esmaili-Gisavandani, H.; Adib, A. Evaluation of climate change effects on flood frequency in arid and semi-arid basins. *Water Supply* **2022**, *22*, 6740–6755. [[CrossRef](#)]
23. Baig, M.F.; Mustafa, M.R.U.; Baig, I.; Takaijudin, H.B.; Zeshan, M.T. Assessment of Land Use Land Cover Changes and Future Predictions Using CA-ANN Simulation for Selangor, Malaysia. *Water* **2022**, *14*, 402. [[CrossRef](#)]
24. Azmat, M.; Liaqat, U.W.; Qamar, M.U.; Awan, U.K. Impacts of changing climate and snow cover on the flow regime of Jhelum River, Western Himalayas. *Reg. Environ. Chang.* **2016**, *17*, 813–825. [[CrossRef](#)]
25. Ahmad, Z.; Hafeez, M.; Ahmad, I. Hydrology of mountainous areas in the upper Indus Basin, Northern Pakistan with the perspective of climate change. *Environ. Monit. Assess.* **2011**, *184*, 5255–5274. [[CrossRef](#)]
26. Anjum, M.N.; Ding, Y.; Shangguan, D.; Liu, J.; Ahmad, I.; Ijaz, M.W.; Khan, M.I. Quantification of spatial temporal variability of snow cover and hydro-climatic variables based on multi-source remote sensing data in the Swat watershed, Hindukush Mountains, Pakistan. *Meteorol. Atmos. Phys.* **2018**, *131*, 467–486. [[CrossRef](#)]
27. Rahman, M.A.; Yunsheng, L.; Sultana, N. Analysis and prediction of rainfall trends over Bangladesh using Mann–Kendall, Spearman’s rho tests and ARIMA model. *Meteorol. Atmos. Phys.* **2016**, *129*, 409–424. [[CrossRef](#)]
28. Zhang, Y.; You, Q.; Chen, C.; Ge, J. Impacts of climate change on streamflows under RCP scenarios: A case study in Xin River Basin, China. *Atmos. Res.* **2016**, *178*, 521–534. [[CrossRef](#)]
29. Almazroui, M.; Islam, M.N.; Saeed, F.; Alkhalaf, A.K.; Dambul, R. Assessing the robustness and uncertainties of projected changes in temperature and precipitation in AR5 Global Climate Models over the Arabian Peninsula. *Atmos. Res.* **2017**, *194*, 202–213. [[CrossRef](#)]
30. Liu, Y.; Fan, K. An application of hybrid downscaling model to forecast summer precipitation at stations in China. *Atmos. Res.* **2014**, *143*, 17–30. [[CrossRef](#)]
31. Xue, Y.; Janjic, Z.; Dudhia, J.; Vasic, R.; De Sales, F. A review on regional dynamical downscaling in intraseasonal to seasonal simulation/prediction and major factors that affect downscaling ability. *Atmos. Res.* **2014**, *147*, 68–85. [[CrossRef](#)]
32. Akhtar, M.; Ahmad, N.; Booij, M. The impact of climate change on the water resources of Hindukush–Karakoram–Himalaya region under different glacier coverage scenarios. *J. Hydrol.* **2008**, *355*, 148–163. [[CrossRef](#)]
33. Iqbal, M.; Wen, J.; Masood, M.; Masood, M.U.; Adnan, M. Impacts of Climate and Land-Use Changes on Hydrological Processes of the Source Region of Yellow River, China. *Sustainability* **2022**, *14*, 14908. [[CrossRef](#)]
34. Haleem, K.; Khan, A.U.; Ahmad, S.; Khan, M.; Khan, F.A.; Khan, W.; Khan, J. Hydrological impacts of climate and land-use change on flow regime variations in upper Indus basin. *J. Water Clim. Chang.* **2021**, *13*, 758–770. [[CrossRef](#)]
35. Mahmood, R.; Jia, S. Assessment of Impacts of Climate Change on the Water Resources of the Transboundary Jhelum River Basin of Pakistan and India. *Water* **2016**, *8*, 246. [[CrossRef](#)]
36. Babur, M.; Babel, M.S.; Shrestha, S.; Kawasaki, A.; Tripathi, N.K. Assessment of Climate Change Impact on Reservoir Inflows Using Multi Climate-Models under RCPs—The Case of Mangla Dam in Pakistan. *Water* **2016**, *8*, 389. [[CrossRef](#)]
37. Mahmood, R.; Jia, S.; Babel, M.S. Potential Impacts of Climate Change on Water Resources in the Kunhar River Basin, Pakistan. *Water* **2016**, *8*, 23. [[CrossRef](#)]
38. Ahmad, I.; Zhang, F.; Tayyab, M.; Anjum, M.N.; Zaman, M.; Liu, J.; Farid, H.U.; Saddique, Q. Spatiotemporal analysis of precipitation variability in annual, seasonal and extreme values over upper Indus River basin. *Atmos. Res.* **2018**, *213*, 346–360. [[CrossRef](#)]
39. Rozenberg, J.; Davis, S.J.; Narloch, U.; Hallegatte, S. Climate constraints on the carbon intensity of economic growth. *Environ. Res. Lett.* **2015**, *10*, 95006. [[CrossRef](#)]

40. Basheer, A.K.; Lu, H.; Omer, A.; Ali, A.B.; Abdelgader, A.M.S. Impacts of climate change under CMIP5 RCP scenarios on the streamflow in the Dinder River and ecosystem habitats in Dinder National Park, Sudan. *Hydrol. Earth Syst. Sci.* **2016**, *20*, 1331–1353. [[CrossRef](#)]
41. Diaz-Nieto, J.; Wilby, R.L. A comparison of statistical downscaling and climate change factor methods: Impacts on low flows in the River Thames, United Kingdom. *Clim. Chang.* **2005**, *69*, 245–268. [[CrossRef](#)]
42. Anandhi, A.; Frei, A.; Pierson, D.C.; Schneiderman, E.M.; Zion, M.S.; Lounsbury, D.; Matonse, A.H. Examination of change factor methodologies for climate change impact assessment. *Water Resour. Res.* **2011**, *47*. [[CrossRef](#)]
43. Zhang, Y.; Su, F.; Hao, Z.; Xu, C.; Yu, Z.; Wang, L.; Tong, K. Impact of projected climate change on the hydrology in the headwaters of the Yellow River basin. *Hydrol. Process.* **2015**, *29*, 4379–4397. [[CrossRef](#)]
44. Moriasi, D.N.; Arnold, J.G.; Van Liew, M.W.; Bingner, R.L.; Harmel, R.D.; Veith, T.L. Model evaluation guidelines for systematic quantification of accuracy in watershed simulations. *Trans. ASABE* **2007**, *50*, 885–900. [[CrossRef](#)]
45. Kumar, K.S.; Kumari, K.P.; Bhaskar, P.U. Application of Markov chain & cellular automata based model for prediction of Urban transitions. In Proceedings of the 2016 International Conference on Electrical, Electronics, and Optimization Techniques (ICEEOT), Chennai, India, 3–5 March 2016; pp. 4007–4012. [[CrossRef](#)]
46. Tan, M.L.; Ibrahim, A.L.; Yusop, Z.; Chua, V.P.; Chan, N.W. Climate change impacts under CMIP5 RCP scenarios on water resources of the Kelantan River Basin, Malaysia. *Atmos. Res.* **2017**, *189*, 1–10. [[CrossRef](#)]
47. Yang, T.; Hao, X.; Shao, Q.; Xu, C.-Y.; Zhao, C.; Chen, X.; Wang, W. Multi-model ensemble projections in temperature and precipitation extremes of the Tibetan Plateau in the 21st century. *Glob. Planet. Change* **2012**, *80*, 1–13. [[CrossRef](#)]
48. Yan, L.; Liu, Z.; Chen, G.; Kutzbach, J.E.; Liu, X. Mechanisms of elevation-dependent warming over the Tibetan plateau in quadrupled CO₂ experiments. *Clim. Change* **2016**, *135*, 509–519. [[CrossRef](#)]
49. You, Q.; Min, J.; Kang, S. Rapid warming in the Tibetan Plateau from observations and CMIP5 models in recent decades. *Int. J. Clim.* **2015**, *36*, 2660–2670. [[CrossRef](#)]
50. Dimri, A.; Kumar, D.; Choudhary, A.; Maharana, P. Future changes over the Himalayas: Maximum and minimum temperature. *Glob. Planet. Chang.* **2018**, *162*, 212–234. [[CrossRef](#)]
51. Xin, J.; Gong, C.; Wang, S.; Wang, Y. Aerosol direct radiative forcing in desert and semi-desert regions of northwestern China. *Atmos. Res.* **2016**, *171*, 56–65. [[CrossRef](#)]
52. Ozturk, T.; Turp, M.T.; Türkeş, M.; Kurnaz, M.L. Projected changes in temperature and precipitation climatology of Central Asia CORDEX Region 8 by using RegCM4.3.5. *Atmos. Res.* **2017**, *183*, 296–307. [[CrossRef](#)]
53. Shamir, E.; Megdal, S.B.; Carrillo, C.; Castro, C.L.; Chang, H.-I.; Chief, K.; Corkhill, F.E.; Eden, S.; Georgakakos, K.P.; Nelson, K.M.; et al. Climate change and water resources management in the Upper Santa Cruz River, Arizona. *J. Hydrol.* **2015**, *521*, 18–33. [[CrossRef](#)]
54. Kaskaoutis, D.; Houssos, E.; Solmon, F.; Legrand, M.; Rashki, A.; Dumka, U.; Francois, P.; Gautam, R.; Singh, R. Impact of atmospheric circulation types on southwest Asian dust and Indian summer monsoon rainfall. *Atmos. Res.* **2018**, *201*, 189–205. [[CrossRef](#)]
55. Wang, C. Impact of anthropogenic absorbing aerosols on clouds and precipitation: A review of recent progresses. *Atmos. Res.* **2013**, *122*, 237–249. [[CrossRef](#)]
56. Immerzeel, W.W.; Pellicciotti, F.; Bierkens, M.F.P. Rising river flows throughout the twenty-first century in two Himalayan glacierized watersheds. *Nat. Geosci.* **2013**, *6*, 742–745. [[CrossRef](#)]

Disclaimer/Publisher’s Note: The statements, opinions and data contained in all publications are solely those of the individual author(s) and contributor(s) and not of MDPI and/or the editor(s). MDPI and/or the editor(s) disclaim responsibility for any injury to people or property resulting from any ideas, methods, instructions or products referred to in the content.